Applied Geochemistry

Biomarkers Thermal Maturity Parameters in Bitumen as a Proxy for Seismic vs. Aseismic Mirror-like Fault Surfaces

--Manuscript Draft--

Manuscript Number:	APGEO-D-26-00971
Article Type:	Research Paper
Keywords:	seismic slip; aseismic slip; faults; fault mirror; biomarkers; thermal maturity
Corresponding Author:	Miriana Chinello University of Bergen
First Author:	Miriana Chinello, PhD
Order of Authors:	Miriana Chinello, PhD
	Andrea Schito, PhD
	Stephen Bowden, PhD
	Elena Spagnuolo, PhD
	Stefano Aretusini, PhD
	Telemaco Tesei, PhD
	Giulio Di Toro, PhD
Abstract:	Mirror-like Surfaces (MSs) are ultra-polished fault surfaces that experimental studies have shown can form during seismic and aseismic deformation (slip rates ≈1 m/s vs. <0.0001 m/s). To determine which MSs form during seismic (rapid temperature increase) or aseismic (negligible temperature increase) slip along the fault, we measured sterane and hopane thermal maturity parameters in bituminous MSs and their underlying slip zone. Samples with MSs were taken from faults hosted in bituminous dolostones from the Central Apennines, Italy, with displacements ranging from millimeters to meters. To support interpretation of the naturally formed MSs, thermal maturity was also assessed for experimental MSs obtained at seismic (1 to 3 m/s) and sub-seismic (0.0001 m/s) slip rates, and for powders statically heated at 400 °C for 2 seconds up to 12 hours. Higher thermal maturity in MSs with respect to the associated slip zone were measured in most of the natural MSs and in the “seismic” experimental MSs. For static-heating experiments, heating at less than 30 seconds was sufficient to change concentrations of biomarkers, while heating for more than 60 seconds was needed to increase sterane 20S and hopane 22S thermal maturity parameters. We show that sterane 20S and hopane 22S parameters have different friction- and burial-induced thermal maturation pathways. We conclude that, with respect to “aseismic” MSs, rapid temperature increase during earthquakes can locally alter biomarkers and increase thermal maturity in “seismic” fault Mirror-like Surfaces.

Biomarkers Thermal Maturity Parameters in Bitumen as a Proxy for Seismic vs. Aseismic Mirror-like Fault Surfaces

M. Chinello[1,2*], A. Schito[3,4,5], S. A. Bowden[4], E. Spagnuolo[6], S. Aretusini[6], T. Tesei[2], and G. Di Toro[2,6]

[1] Department of Earth Science, University of Bergen (UiB), Allégaten 41, 5007 Bergen, Norway

[2] *Dipartimento di Geoscienze, Università degli Studi di Padova*, Padua, Italy

[3] Department of Mineralogy, Petrology and Applied Geology, *Facultat de Ciències de la Terra, Universitat de Barcelona, Carrer Marti i Franques s/n*, 08028, Barcelona, Spain

[4] Department of Geology and Geophysics, University of Aberdeen, Aberdeen AB24 3UE, UK

[5] *Institut de Recerca Geomodels, Facultat de Ciències de la Terra, Universitat de Barcelona, Carrer Martí i Franquès s/n*, 08028 Barcelona, Spain

[6] *Istituto Nazionale di Geofisica e Vulcanologia* (INGV), Rome, Italy

Corresponding author: Miriana Chinello (miriana.chinello@uib.no)

Key Points:

- Experimental and natural mirror-like fault surfaces may have higher thermal maturity of biomarkers than the surrounding rocks
- Static heating at 400°C for 30-60 s can increase concentration and values of sterane and hopane biomarkers
- Sterane and hopane biomarkers can detect frictional heat pulses occurring in "seismic" Mirror-like Surfaces

Abstract

Mirror-like Surfaces (MSs) are ultra-polished fault surfaces that experimental studies have shown can form during seismic and aseismic deformation (slip rates ≈1 m/s vs. <0.0001 m/s). To determine which MSs form during seismic (rapid temperature increase) or aseismic (negligible temperature increase) slip along the fault, we measured sterane and hopane thermal maturity parameters in bituminous MSs and their underlying slip zone. Samples with MSs were taken from faults hosted in bituminous dolostones from the Central Apennines, Italy, with displacements ranging from millimeters to meters. To support interpretation of the naturally formed MSs, thermal maturity was also assessed for experimental MSs obtained at seismic (1 to 3 m/s) and sub-seismic (0.0001 m/s) slip rates, and for powders statically heated at 400 °C for 2 seconds up to 12 hours. Higher thermal maturity in MSs with respect to the associated slip zone were measured in most of the natural MSs and in the "seismic" experimental MSs. For static-heating experiments, heating at less than 30 seconds was sufficient to change concentrations of biomarkers, while heating for more than 60 seconds was needed to increase sterane 20S and hopane 22S thermal maturity parameters. We show that sterane 20S and hopane 22S parameters have different friction- and burial-induced thermal maturation pathways. We conclude that, with respect to "aseismic" MSs, rapid temperature increase during earthquakes can locally alter biomarkers and increase thermal maturity in "seismic" fault Mirror-like Surfaces.

1 Introduction

During the seismic cycle, faults can experience seismic slip rates (>0.0001 m/s) as well as aseismic to sub-seismic slip rates (<0.0001 m/s) or fault locking during the pre-seismic, post-seismic and inter-seismic phases (Rowe and Griffith, 2015; Scholz, 2019). Several fault-zone rock types and rock microstructures have been linked to seismic slip, among which Mirror-like Surfaces (MSs) have been proposed as markers of seismic deformation and associated with dynamic weakening in carbonates (Fondriest et al., 2013; Siman-Tov et al., 2013). MSs are ultra-polished fault surfaces that reflect light and are characterized by a sub-micrometric-scale roughness (Siman-Tov et al., 2013). MSs are most commonly observed in seismogenic fault zones, cutting carbonate rocks exhumed from shallow depth (Hancock and Barka, 1987; Jackson and McKenzie, 1999; Fondriest et al., 2012; 2013; 2015; Siman-Tov et al., 2013; Demurtas et al., 2016; Leah et al., 2018; Ohl et al., 2020; Chinello et al., 2023; Cortinovis et al., 2024; Koppensteiner et al., 2025; Agosta et al., 2026). Experimental studies on limestone and dolostone have produced MSs by shearing both gouges and intact rock samples over a wide range of slip conditions, from seismic (>0.1 m/s; Han et al., 2010; Boneh et al., 2013; Fondriest et al., 2013; Smith et al., 2013; Siman-Tov et al., 2015; Spagnuolo et al., 2015; De Paola et al., 2015; Pozzi et al., 2018; Park et al; 2021; Demurtas et al., 2021; Rempe et al., 2020; Cornelio et al., 2024; Chinello et al., under review) to sub-seismic (≈0.1–100 µm/s; Verberne et al., 2014; Tesei et al., 2017; Passelègue et al., 2019; Aubry et al., 2020; Chinello et al., under review) slip rates. These experimental observations indicate that MSs in carbonates may be produced by both fast (seismic) and slow (aseismic) deformation processes. These experimental observations confirm that the MSs present in carbonates can be generated by both rapid (seismic) and slow (aseismic) deformation processes. It is therefore necessary to identify methods that allow us to distinguish between these processes, also for evaluating the seismic hazard associated with active faults.

During seismic slip, fault frictional heating causes an abrupt rise in temperature that can reach up to 1250 °C in carbonates (Aubry et al., 2020; Aretusini et al., 2021b). This temperature increase is sufficient to induce decarbonation and to activate thermally driven deformation mechanisms and processes that weaken the fault (Han et al., 2007; 2010; De Paola et al., 2011; 2015; Tisato et al., 2012; Niemeijer et al., 2012; Smith et al., 2013; Rempe et al., 2014; 2020; Spagnuolo et al., 2015; Pozzi et al., 2019; Nielsen et al., 2021; Rempe et al., 2020; Demurtas et al., 2016; 2021; Cornelio et al., 2024; Curzi et al., 2026). The temperature increase associated with seismic slip can also increase thermal maturity of organic matter (e.g., Polissar et al., 2011; Savage et al., 2014). Thermal maturation refers to the progress of irreversible temperature- and time-dependent chemical reactions that alter organic matter (Peters et al., 2005). In sedimentary basins, during thermal maturation and after the initial stages of diagenesis, solid organic matter thermally decomposes and forms bitumen from kerogen (Tissot and Welte, 1984). At higher levels of thermal maturation, the structure of organic matter reorders towards a more thermodynamically stable configuration in the so-called graphitization stage (Buseck and Beyssac, 2014). A number of indicators can be used to measure and quantify thermal maturation, with the most robust being those supported by kinetic models that relate measurements to both the duration and temperature of heating. Such indicators include vitrinite reflectance (Ro%) and certain biomarker thermal maturity parameters, which track changes in the relative abundances of stereoisomers of thermally sensitive organic molecules preserved in sedimentary rocks (Figure 1; Mackenzie and McKenzie, 1983; Sweeney and Burnham, 1990; Peters et al., 2005). Thermal maturity is also widely applied to investigate natural phenomena involving different heat sources and heating rates, such as within the thermal aureoles of magmatic intrusions, wildfires, contact and impact metamorphism, and frictional heating (see Schito et al., 2023 for a review). However, these approaches are valid only within specific temperature-time ranges and their applicability requires further calibration.

Several studies have investigated the thermal maturity and/or maximum temperature associated with coseismic frictional heating during the shearing of natural and experimental organic-rich fault rocks and gouges, by mean of Vitrinite reflectance (Bustin, 1983; Suchy et al., 1997; O'Hara, 2004; 2006; Sakaguchi et al., 2011; Kitamura et al., 2012; Furuichi et al., 2015), Raman and IR spectroscopy (Hirono et al., 2015; Furuichi et al., 2015; Kaneki et al., 2016; Ito et al., 2017; Kuo et al., 2017; Henry et al., 2019; Fan et al., 2020; Morozov et al., 2020; Kedar et al., 2020; Muirhead et al., 2021), and molecular markers (i.e., biomarkers; Polissar et al., 2011; Savage et al., 2014; 2018; Sheppard et al., 2015; Coffey et al., 2019; Savage and Polissar, 2019; Rabinowitz et al., 2020). Among these, Kitamura et al., (2012), Sheppard et al., (2015) and Rabinowitz et al., (2017) applied kinetics models of Vitrinite reflectance and selected biomarkers (i.e., methylphenanthrenes, alkenones and n-alkanes) to determine the thermal conditions generated within faults by earthquakes. These measurements can be applied to perform bulk (i.e., biomarkers) or punctual analyses with a microscope on a specific clast, grain, or rock component (i.e., Raman and IR spectroscopy). The smaller the volume measured the better the capacity to resolve non-uniform heat distribution at the microscale (McDermott et al., 2017; Calzolari et al., 2020). By sampling small volumes molecular marker analyses can also emulate punctual measurements (Savage and Polissar, 2019). In all cases, a proper temperature calibrated kinetic model is needed for the heating environment concerned so that measurements of thermal maturity can be linked to temperature and duration of heating (Kaneki et al., 2016; Ito et al., 2017; Schito et al., 2022; Schito et al., 2023).

In this work, we investigate the potential of hopane and sterane biomarker thermal maturity parameters to record temperature increases caused by frictional heating in faults during seismic slip. Our aim is also to determine the seismic or aseismic origin of MSs in faults cutting bituminous dolostones in the Italian Central Apennines (Chinello et al., 2023). In addition to observations of naturally faulted samples, the ability of the hopane 22S and sterane 20S biomarkers to record short-lasting heat pulses is investigated by (1) statically-heating bituminous dolostone powders at 400°C for increasing time periods and (2) shearing bituminous dolostones powders at seismic (1-3 m/s, temperature increase of ≈350°C) and sub-seismic (0.0001 m/s, negligible temperature increase) slip rates. How biomarker parameters can be used to assess thermal alteration of natural Mirror-like Surfaces is then investigated.

2 Geological setting

The out-of-sequence Monte Camicia Thrust is a ≈30° WSW-dipping fault exhumed from ≈3 km depth located in the Fornaca Valley of the Gran Sasso Massif in the Italian Central Apennines (Figure 2a). The thrust is part of the Gran Sasso Thrust System that was active between the Messinian and early-middle Pliocene during the formation of the Apennine fold and thrust belt (Ghisetti and Vezzani, 1986; Ghisetti, 1987; Ghisetti and Vezzani, 1991; Lucca et al., 2019; Chinello et al., 2023). Field, structural, and isotopic evidence suggests that the Monte Camicia Thrust was locally reactivated as a normal fault during the extensional gravitational collapse of the Gran Sasso Thrust System that began in the Late Messinian and is still active (Leah et al., 2018; Lucca et al., 2019).

The bituminous dolostones (*Dolomie Bituminose* Fm., Upper Triassic) outcrop in the footwall of the thrust and are characterized by mm-dm thick beds of organic matter-rich dolostones (grey to black in color) interbedded with up to 10 m thick dolostone beds (Adamoli et al., 1984; Barchi and Bigozzi 1995; Figure 2b). The bituminous dolostones can have up to 40% of total organic carbon content (Katz et al., 2000) and, based on apatite fission track and vitrinite reflectance analyses by Rusciadelli et al. (2005), experienced maximum temperature of 100°C during burial.

In the southernmost part of the Fornaca Valley, several NE-SW and E-W striking normal faults cut through the bituminous dolostones in the footwall of the Monte Camicia Thrust with dip-slip to transtensional kinematics, accommodating a few mm to a few m of displacement (Figure 2a). These faults comprise ultra-cataclastic slip zones bound by Mirror-like Surfaces (MSs), often decorated by smeared pre-oil solid bitumen (Figure 2b). Microstructural investigations revealed that these slip zones record the main phases of the seismic cycle (Chinello et al., 2023). Aseismic deformation was accommodated by viscous flow of bitumen, cataclastic flow and pressure solution, whereas the presence of fragments of older slip zones and bitumen-rich clasts cemented by calcite suggests the occurrence of seismic ruptures in the presence of carbonate-rich fluids followed by post-seismic or inter-seismic fault sealing (Chinello et al., 2023). MSs are extremely common in the area and are also found in faults with negligible displacement (< 1 mm). At the microscale MSs consist of dolomite nanoparticles and smeared bitumen (Figure 2b, c; Chinello et al., 2023).

3 Materials and Methods

3.1 Natural samples

Analyzed natural samples include (Supp. Table S1): slip zones containing MSs from faults with displacement ranging from 0.001 m to 11.22 m (samples 2, 3, 7, 8, 9), a natural MS belonging to a folded bedding interface (sample 6), and the undeformed Host Rock (HR; bituminous dolostones).

3.2 Powder preparation, rotary-shear and static-heating experiments

To provide materials for the experiments, host rock samples of bituminous dolostones collected tens of meters from the main faults were ground within a disc mill and sieved to obtain a bituminous dolostone powder with grain size <250 µm. Rotary-shear experiments were performed on the powders with the apparatus SHIVA (Di Toro et al., 2010) at HP-HT laboratory of INGV in Rome by imposing on the bituminous dolostone powder sub-seismic (0.0001 m/s) and seismic (1 and 3 m/s) slip rates under a normal stress of 20 MPa and room-humidity conditions (for description of the experiments see Chinello et al., under review). Nine static-heating experiments were conducted on powders heated in an oven at 400 °C for increasing time periods. This temperature was chosen because it is similar to that measured by the thermocouple during the "seismic" rotary-shear experiments (temperature increase ≈350 °C; Chinello et al., under review). Heating experiments were conducted at the HP-HT laboratory of INGV in Rome and at the Department of Geosciences of the University of Padua. A crucible was pre-heated at 400 °C for about ten minutes (until the temperature stabilized inside the oven), then it was removed, filled with 2 g of bituminous dolostone powder and returned to the oven for the selected time interval. The same procedure was repeated 9 times for progressively longer heating times (2 s, 10 s, 30 s, 1 min, 5 min, 20 min, 1 h, 3 h, 12 h; Supp. Table S2). After heating, the crucible was quenched in water at ambient temperature.

3.3 Biomarker thermal maturity analysis

Thermal maturity analyses of bitumen using biomarkers were conducted on (i) "undeformed" host rock (Figure 2a), (ii) natural slip zone samples containing a MS (Figure 2b, c), (iii) powders collected after the static-heating experiments, and (iv) artificial slip zone samples containing a MS produced in rotary-shear experiments (Figure 2d, e). The biomarkers selected for the thermal maturity analysis where (i) sterane 20S, (ii) $\%\alpha\beta\beta$ sterane, (iii) hopane 22S, and *(iv)* $\beta\beta$ hopane (see Supporting Information for details). Prior to selecting biomarkers, we attempted to measure thermal maturity with MicroRaman spectroscopy as a non-destructive and punctual technique. However, a very high background fluorescence was sufficient to obscure key Raman bands used to assess the thermal maturity of organic matter (see Supporting Information for details).

3.3.1 Bitumen extraction

To provide duplicate observations samples were divided into "A" and "B" subsamples (step 1 in Figure 3a). Bitumen was extracted from both parts using the same techniques. For compact and cohesive samples, extraction occurred by placing a sample with the MS "face down" in a 5 mm deep layer of dichloromethane ("DCM"; CH_2Cl_2) and sonicating it for three minutes. Instead, for friable and weak samples, the specimen was held over a beaker using a pair of tweezers and the surface was rinsed with 2 ml of DCM (step 2 in Figure 3a). After the extraction of bitumen from the MS, the slip zone ("SZ") containing the MS was separated with a saw from the rest of the sample, which could be analyzed as a "control" for its respective sample ("C"; Step 3 in Figure 3a). Both the "SZ" and "C" parts were then crushed using a small pestle and mortar (Step 4 in Figure 3a), and the resulting powders were soaked in DCM and Hexane in multiple steps for bitumen extraction by sonication in ultrasound baths (Step 5 in Figure 3a). Extracts from the "SZ" and "C" parts were separated into saturated, aromatic, and polar fractions by silica-gel flash-chromatography. In this way, each natural sample was represented by two subsamples labelled "A" and "B". This potentially yielded a maximum of six observations for each natural sample (2 x "MS", 2 x "SZ", and 2 x "C"; Supp. Table S1). For samples 2, 3 and 5 only the control part of sample A was measured. For sample 8 the control part was not separated from the slip zone because it was the first sample to be analyzed, and the methodology had not been fully developed at that point.

Bitumen from powders after the static-heating experiments and from the undeformed natural samples was obtained with a single bulk extraction ("Bu" in Supp. Tables S1 and S2), following only steps 4 and 5 for the undeformed natural samples, and only step 5 for the heated powders (Figure 3a). Bitumen from samples produced during rotary-shear experiments was extracted following only steps 2, 4 and 5: samples were too small to be divided into subsamples "A" and "B" and too thin and friable to separate "SZ" and "C" parts (samples were ≈1.5 mm thick).

3.3.2 Gas Chromatography Mass Spectrometry analysis of bitumen for biomarkers

Gas Chromatography Mass Spectrometry (GC-MS) was performed at the Department of Geology and Geophysics, University of Aberdeen (Scotland, UK) using an Agilent Technologies 8890 N Gas Chromatograph (GC) fitted with a HP-5ms UI column (30 m length, 2.5 mm ID, 0.25 µm film thickness) and connected to 5977 MSD EI Mass Spectrometer (MS) operating in SIM (Selected Ion Monitoring) mode. Samples were injected using a split/splitless injector operating in spitless mode. Oven temperature was hold at 60 °C for 2 min rising to 120 °C at 20 °C /min then to 290 °C at 4 °C /min and held at 290 °C for 27.5 min. The SIM mode had 22 ions each with a dwell time of 40 ms. Quantification of hopane and sterane biomarkers was performed relative to an internal standard of d4 C27 ααα (20R)–Cholesterane, added after bitumen extraction or column chromatography.

Steranes and hopanes biomarkers were identified based on their relative retention times and by comparison to well-characterized samples. Peak heights and areas were measured using the following ion chromatograms: the m/z 217 for steranes (Figure 3b) and m/z 191 for hopanes (Figure 3c). Data analysis was performed using MSD ChemStation G1701DA

D.02.00.275 software (Agilent Technologies). To check for variations resulting from manual fitting of baselines to peaks, all measurements of biomarkers parameters and data are an average of the replicates.

Sterane and hopane biomarker thermal maturity parameters and yields of the relative S and R isomers are presented in Supp. Tables S1 and S2. These parameters are formulated after Farrimond et al. (1998) that also presents context for pre-oil window ("immature" stage) thermal maturation of steranes and hopanes (see Supporting Information for an in-detail description; Figure 1). Extraction yields (ng/g of rock) are calculated as concentrations relative to d4 Cholestane and are not absolute concentrations. In each case the point of reference (mass of rock) is the mass of the split sample (e.g. the A or B subsample), prior to division into the MS, SZ and C subsamples (Figure 3a), thus the MS is treated as the first stage in a sequential extraction of the slip zone (see Supporting Information for an in-detail description).

Signal-to-noise ratios were determined following the standard chromatographic approach commonly applied for GC–MS studies (Felinger, 2011), in which the signal corresponds to peak height (or area) and the noise is estimated by measuring peaks in an adjacent but low-signal region of the chromatogram. This procedure is widely used in conventional GC–MS quantification, trace compound detection, and biomarker analysis because it accounts for both matrix-derived noise (e.g. compounds generating interfering ionizations or detector signals), as well as instrumental and procedural noise (Peters et al., 2005). Signal-to-noise ratios for measurements of the S-isomer and its effect on the calculation of the sterane 20S and hopane 22S parameters, are reported in Supp. Table S3 for a set of representative samples selected by visual inspection of the ion chromatograms. Signal-to-noise ratios were most favorable for the hopane 22S parameter, corresponding to an error $< \pm 2\%$ for the analysis of both natural slip zone samples and experimental samples. In contrast, signal-to-noise ratios for the sterane 20S parameter were less favorable for the experimental samples, reflecting the small size of the sterane 20S peak in the chromatograms, and corresponded to errors $> \pm 3\%$. For natural slip zone samples, sterane 20S signal-to-noise ratios corresponded to an error $< \pm 2\%$. Errors were not systematically greater for MSs than for the slip zone or control part; however, for the sterane 20S parameter, MSs samples from faults with limited displacement exhibited the largest errors. When expressed as absolute uncertainty in the hopane 22S and sterane 20S parameters, signal-to-noise ratios correspond to an error of ≈ 0.01 in most cases (Supp. Table S3). In Supp. Tables S1 and S2, where the differences between replicate measurements corresponded to $\sigma = 0$, the error was conservatively set to $\sigma = 0.01$.

4 Results

4.1 Thermal maturity of the host rock and natural MS-samples

In the host rock, sterane 20S and hopane 22S parameters are 0.07±0.01 and 0.30±0.01, respectively. Sterane and hopane yields are similar, ranging from 3.04 to 42.77 ng/g (Figures 4, 5, Supp. Tables S1-S2).

<u>Sterane 20S</u> parameter in the MS of sample 8 (displacement 0.87 m) is significantly higher than in the corresponding slip zone for both part A and B (Figure 4g). Higher sterane 20S

values in the MS relative to the slip zone and control part are also measured in samples 2B, 3B and 9B (displacement of 0.01, 0.05 and 1.23 m respectively) and in 6A-6B where the MS is located on a bedding surface within the limb of a fold (i.e., displacement ≈0 m). In sample 9A, the sterane 20S value in the MS is similar to that in the associated slip zone, but slightly higher than in the control part. In contrast, samples 3A, 5, 6A and 7 show no significant differences in sterane 20S values among the MS, slip zone and control part, with values ranging from 0.06 to 0.10. In sample 6A, the control part is slightly more mature than the slip zone. Sterane 20S and 20R isomer concentrations in the MSs are generally low (0-12.85 ng/g) when compared with slip zone and control samples. This is mainly because biomarkers in the MSs represent only a small volume of the whole sample (i.e., only the MS and a small surrounding depth of the sample were permeated and extracted). In contrast, samples 8 and 9 exhibit higher values of the Sterane 20S parameter in the MS and similar concentrations of steranes between the MS and the slip zone. Concentrations in the slip zone and in the control part are generally similar, or slightly lower in the slip zone (Figure 4a, c, e). However, in samples 6, 7B and 9A concentrations are lower in the control part.

Hopane 22S parameter has a similar pattern to that of sterane 20S (Figure 5g). In sample 8, the hopane 22S value in the MS is higher than in the associated slip zone for both parts A and B. A higher value of the hopane 22S parameter in the MS relative to the associated slip zone and control part are also measured in 6A, 2B, 3B, 9B and 7B (displacements of 0, 0.001, 0.05, 1.23, 11.22 m, respectively). For samples 7A and 9A, the value of the hopane 22S parameter in the MS is higher than in the slip zone; however, the control part shows values similar to or higher than those of the MS. Measurement uncertainties for the hopane 22S parameter are relatively large in sample 5; therefore, this sample is excluded from further analysis. No significant differences among the MS, slip zone and control part are observed in samples 2A and 3A. Hopane 22S and 22R isomer concentrations in the MSs are generally lower than slip zones with the exceptions of samples 2B, 8 and 9 which display similar concentrations of hopanes between the MS and the slip zones (Figure 5b, d, f). Some slip zone samples have higher concentrations of hopanes than the associated control samples (i.e., samples 6B, 7B and 9A).

The average thermal maturity values of all the control samples (i.e., part C of each subsample; Figure 3) are 0.08 for sterane 20S and 0.26 for hopane 22S (Figures 4g, 5g). These values fall within the analytical uncertainty of the sterane 20S and hopane 22S parameter values of the host rock sample (Supp. Table S1). No correlation is observed between thermal maturity values and the total displacement accumulated along the sampled faults (from 0.05 m to 11.22 m; Figures 4g, 5g).

4.2 Thermal maturity of the starting powder and experimental samples

Thermal maturity of bitumen in the starting powder and in the shear- and static-heating experimental samples is assessed using the sterane 20S, the *%αββ* sterane, the hopane 22S and the *ββ* hopane parameter (Supp. Table S2; Figures 4h, 5h), and the relative concentrations of the sterane and hopane S and R isomers (Supp. Table S2; Figure 4b, d, f; Figure 5b, d, f). In the starting powder the sterane 20S and hopane 22S values are 0.07±0.01 and 0.27±0.02, respectively. These values for the starting powder are within measurement error of the average sterane 20S and hopane 22S values of the control samples (see section 4.1 and Figures 4g, 5g). For the starting powder, *%αββ* sterane value is 0.27±0.02 and *ββ* hopane value is 0.13±0.02. Concentrations for steranes and hopanes are 36.5-139309.9 ng/g.

4.2.1 Static-heating experimental samples

Sterane 20S is similar to that of the starting powder for heating durations shorter than 1 minute. Then, sterane 20S increases with time from 0.15±0.02 after 5 minutes to 0.57±0.02 after 1 hour (Figure 4h).

%αββ sterane has similar trend to Sterane 20S (Supp. Table S2). Although, thermal maturity does not change significantly for experiments heated less than 5 minutes, yields of sterane 20S and 20R isomers initially decline to 10.48-170.54 ng/g after heating for 10 seconds, then rise after 30 seconds of heating and finally fall to 0.11-0.14 ng/g after heating for 1 hour (Figure 4f; Supp. Table S2). Steranes are not detected in samples heated for longer.

Hopane 22S is 0.19 to 0.28 for heating durations shorter than 30 seconds, similar to the one of starting powder. Then, the hopane 22S increases from 0.41±0.01 after 1 minute to 0.55±0.01 after 20 minutes (Figure 5h).

ββ hopane, decreases with heating, little in the first 10 seconds, and down to 0.04±0.01 after 20 minutes of heating (Supp. Table S2). Yields of hopane 22S and 22R isomers first decrease to 59.35-254.70 ng/g during heating for 2-10 seconds and then increase after 30 seconds (Figure 5f; Supp. Table S2). After heating for 1 hour, concentration decreases to 0.10 ng/g.

4.2.2 Rotary-shear experimental samples

Sterane 20S in the samples after the experiments performed at seismic slip rates (1 m/s, s1950; 3 m/s, s1952) is higher in the MS than in the underlying slip zone, with MSs values higher than those of the starting powder (Figure 4h). In the sample after the experiment performed at sub-seismic slip rate (0.0001 m/s, s1951), the sterane 20S value of the MS is slightly higher than that of the associated slip zone. However, both values lie within the analytical uncertainty of the starting powder (Figure 4h). Overall, the highest sterane 20S values are measured in the MSs produced at seismic slip rates.

%αββ sterane has a minor increase in thermal maturity (0.01–0.02) between MS and slip zone values across all experiments, regardless of slip rate, and these differences fall within analytical uncertainty of the starting powder (Supp. Table S2). MSs have similar concentrations of sterane 20S isomer to starting values, but slightly lower concentrations of the 20R isomer (Figure 4b, d; Supp. Table S2). Concentrations of the sterane 20S and 20R isomers in the MS and the associated slip zone are similar in the “seismic” experiment at 1 m/s (s1950), slightly lower in the slip zone of the “sub-seismic” experiment (s1951), and higher in the slip zone of the “seismic” experiment with the highest slip rate (3 m/s; s1952).

Hopane 22S in the sample after the experiment performed at 1 m/s (s1950) is higher in the MS obtained than in the underlying slip zone or the starting powder, with the same relative differences found in the experiment performed at 0.0001 m/s (s1951; 0.30±0.02 vs 0.19±0.01;

Figure 5h). In the experiment performed at 3 m/s (s1952), hopane 22S is higher in the MS with respect to the slip zone, but both are lower than the one of the starting powder.

ββ hopane has similar values, within analytical uncertainty, for the MS and the corresponding slip zone, independently of the seismic vs. sub-seismic loading conditions imposed in the experiments (Supp. Table S2). Compared to the starting powder, lower concentrations of hopane 22S and 22R isomers are observed in the MSs produced at 1 m/s and 0.0001 m/s, while yields are a little higher in the MS produced at 3 m/s (Figure 5b, d; Supp. TableS2). Concentrations of hopane 22S and 22R isomers in the MS relative to the associated slip zone are similar to what is observed for steranes (see above).

5 Discussion

5.1 Bitumen characterization in Dolomie Bituminose *Fm.*

The analyzed host rock sample and starting powder have a low thermal maturity corresponding to 0.07±0.01 for the sterane 20S parameter and 0.27±0.02/0.30±0.02 for the hopane 22S parameter (Figures 1, 4g-h, 5g-h; Supp. Tables S1-S2). The *%αββ* sterane and the *ββ* hopane values of the starting powder are likewise very low (0.27±0.02 and 0.13±0.02, respectively; Supp. Table S2). All parameters are consistent and collectively indicate that the organic matter is immature and corresponds to a pre-oil window "proto-bitumen" or "proto-kerogen" ("immature" stage, Figure 1), confirming that the *Dolomie Bituminose* Fm. is a "very low thermal-maturity bitumen" sensu Curiale (1986). This is also supported by strong fluorescence that obscured Raman signals (see Supporting Information; Lipparini et al. 2021). The thermal maturity in the control part (C) of the analyzed fault rock samples, that is the farthest part from the MS and therefore less affected by frictional heating during slip (Figure 7), can be sometimes slightly higher than the maturity of the host rock (see below), especially for the sterane 20S biomarker (i.e., samples 2A, 3A, 6B, 7A-B, 9A-B; 0.08-0.10 vs. 0.07±0.01; Supp. Table S1), but always within the pre-oil window maturity range ("immature" stage, Figure 1; triangles in Figure 4g).

The faults investigated are associated with the extensional and latest tectonic phase of the Central Apennines. Nevertheless, ours and previous geological investigations in the study area did not observe bitumen as inclusions in veins or in fractures/pores in the stratigraphically upper geological formations or in other lithologies in fault contact with the *Dolomie Bituminose* Fm. (Leah et al., 2018; Lucca et al., 2019). This field evidence, together with the high viscosity of pre-oil solid bitumen (Curiale 1986), indicates that the bitumen extracted from the MSs was not subjected to relevant mobility after diagenesis, but migrated only the minimum distance necessary to reach pores and inter-to intra-fractures in the interbedded dolomite beds and slip surfaces where it is also smeared on the MS (Chinello et al., 2023). Conventional petroleum is therefore absent in host rock and fault zones, implying that the analyzed bitumen faithfully records thermal maturity changes associated with fault deformation. In any case, to mitigate the impact of bitumen migration and the resulting variations in the bitumen's thermal maturity, we compared the biomarkers of the MSs with their respective slip zones (Figure 2).

5.2 Thermal response of the tested biomarkers to short duration heating

5.2.1 The effect of the exposure time during experiments

In static-heating experiments, sterane 20S and hopane 22S parameters detect an increase in thermal maturity after only 1-5 minutes of exposure at 400 °C relative to the starting powder (0.15±0.02 vs 0.07±0.01 for sterane 20S after 5 minutes; 0.41±0.01 vs 0.27±0.02 for hopane 22S after 1 minute; Figures 4h, 5h). These rapid changes occurred over much shorter heating durations than those reported for typical sedimentary basin burial conditions (Mackenzie and McKenzie, 1983; Polissar et al., 2011). Thermal maturity increases progressively with exposure time for both parameters, reaching 0.57±0.02 for sterane 20S after 1h and 0.55±0.01 for hopane 22S after 20 minutes (Figure 4b, d; Supp. Table S2). In the setting of burial diagenesis sterane 20S values of 0.55 correspond to peak oil window conditions (Figure 1), consistent with the behavior of the *%αββ* sterane parameter, which shows little variation until heating duration exceeds 20 minutes (maximum value of 0.55 ± 0.01; Supp. Table S2). The correspondence between maximum values of sterane 20S and *%αββ* sterane parameters and declining biomarker concentrations is consistent with observations of thermal alteration from burial diagenesis and from thermal aureoles around igneous intrusions (Bishop and Abbot, 1995; Farrimond et al., 1998). As expected, the hopane 22S parameter reaches its maximum value earlier than sterane 20S, in agreement with its known maturation behavior prior to peak oil generation (Mackenzie and McKenzie, 1983; Bishop and Abbott, 1993; Farrimond et al., 1998; Peters et al., 2005).

Concentrations of both sterane and hopane S and R isomers decreased during the first 10 seconds of heating, increased after 30 seconds of heating likely reflecting breakdown of macromolecules and generation of new hopanes and steranes, and significantly decreased after 1-5 minutes of heating (Figures 4h, 5h; Supp. Table S2). Hopanes and steranes were not measured in samples heated for longer than 1 h (Supp. Table S2). Therefore, heating for short durations at 400°C results in distinct stages in which concentrations initially decline, then rise and recover as new hopanes and steranes form from the breakdown of geomacromolecules and finally approach zero in a way similar to longer duration heating (Bishop and Abbot, 1995; Farrimond et al., 1998). Notable is that very short duration heating at 400°C reduces concentrations of hopanes and steranes (e.g. they are destroyed) but need not change the sterane 20S and hopane 22S parameters, until heating is sustained for longer. This may have consequences for the sterane 20S and hopane 22S parameters because the increase of both parameters is due to the relative enrichment of one isomer over another (i.e., relative enrichment of the more thermally stable 20S or 22S isomer compared to the biologically-inherited 20R or 22R stereochemistry; MacKenzie et al., 1980; Kolaczkowska et al., 1990). This selective enrichment depends on both relative rates of destruction and also generation from the breakdown of geomacromolecules; both kerogen and bitumen contain occluded steranes and hopanes that are released to form their "free" phase counterparts (Bowden et al., 2006). Thus, if very short duration heating only removes a biomarker isomer but does not generate new ones, this may change parameters in ways not seen in longer duration heating.

In rotary shear experiments, sterane 20S and hopane 22S parameters record a higher thermal maturity in all the MSs with respect to the one measured in the associated slip zone

(Figure 4h, 5h; Supp. Table S2). However, sterane and hopane concentrations change little in the MSs, indicating that the increase in both parameters relative to the associated slip zone is unlikely to result from the release of the S isomer from macromolecular organic matter in protobitumen (Bishop and Abbot, 1995). Instead, it more likely reflects isomer interconversion or preferential destruction of the R isomer. In the slip zones of the experiments performed at 0.0001 m/s and 1 m/s, both sterane and hopane S and R isomers show lower concentrations relative to the starting material (Figure 5h; Supp. Table S2). In contrast, the experiment performed at 3 m/s exhibits substantially higher concentrations in the slip zone than other experimental slip zones, suggesting that the generation of new sterane and hopane isomers occurred only in the slip zone at the highest shear rate (Figure 5h; Supp. Table S2). Accordingly, the lower concentrations of sterane and hopane isomers in the corresponding MS may reflect isomer destruction, consistent with observations at similar maturity levels in static-heating experiments (Supp. Table S2), as well as during early stages of burial and heating near igneous intrusions (Bishop and Abbot, 1995; Farrimond et al., 1998).

Overall, sterane 20S and hopane 22S parameters and concentrations measured in short-duration static-heating experiments closely match those observed in the seismic shear experiment performed at 3 m/s. This is reasonable given the maximum temperature measured in both experiments at seismic shear rates was ≈350 °C (Chinello et al., under review), and experimental durations were 1 s and 0.67 s (for the shear rates of 1 and 3 m/s), and thus durations and temperatures are comparable.

5.2.2 Applicability of sterane and hopane parameters to (fault) frictional heating

When evaluating thermal maturity, it is common practice to cross plot two or more thermal maturity parameters such as the sterane 20S and hopane 22S to check for internal consistency (Peters et al., 2005). Plotting the sterane 20S and hopane 22S parameters together, a trend in thermal maturity is observed in both the experimental and natural samples, showing consistency between the two indicators (Figure 6). The data from static-heating experiments (white to red diamonds in Figure 6a) reproduce the trend described by Farrimond et al. (1998) for the transition from pre-oil window to mid-oil window conditions during burial (Figure 1). The non-linearity of the trend is because hopane 22S parameter reaches a maximum value of about 0.55 when the sterane 20S parameter reaches 0.4, reflecting the tendency of hopane 22S to change more rapidly than sterane 20S (Peters et al., 2005; Figure 6a).

Data from rotary-shear experiments have slip zones that follow the trend of Farrimond et al. (1998) corresponding to lower thermal maturity, while the MSs deviate from the trend toward the upper-right, corresponding to higher thermal maturity (Figure 6a). This deviation suggests that the tendency for the hopane 22S parameter to change more rapidly than the sterane 20S parameter, observed for burial-heating, cannot be used to describe also frictional heating.

A similar pattern is observed in natural samples (Figure 6b). Although both MSs and associated slip zones generally show lower sterane 20S values for a given hopane 22S value (e.g. MS of sample 9A: sterane 20S = 0.10, hopane 22S = 0.27), sterane 20S increases more rapidly relative to the trend for burial-heating described by Farrimond et al. (1998), and in the case of sample 8, values of sterane 20S and hopane 22S are comparable. These distinct trends suggest that a maturity increase is observed moving from the slip zone to MS. In addition, the kinetic behavior of the two parameters differs between heating environments and may therefore be used to discriminate between burial and (fault) friction-related heating.

5.3 Frictional heating recorded by thermal maturity increase in natural and experimental MSs

In the natural samples, sterane 20S and hopane 22S indicate significantly higher thermal maturity in the MS of sample 8 (parts A and B) compared to the slip zone, as well as in samples 2B, 6A, and 9B, where differential values are lower (Figures 4, 5). An increase in thermal maturity in the MS relative to the slip zone, detected by only one biomarker, is also observed in samples 3B and 6B (sterane 20S) and 7B (hopane 22S; Figures 4, 5). In other samples, both with lower and higher displacement (2A, 3A, 7A, and 9A), neither parameter records any thermal maturity difference among MS, SZ, and C (Figures 4, 5). The higher thermal maturity recorded in some of the MS with respect to the associated SZ and C parts, is compatible with the highly localized imprints of temperature rise by frictional heating. However, there is no simple correlation between the total displacement accumulated by each fault and the thermal maturity values. Biomarker yields, on the other hand, can offer some clues.

In samples where the MS and the slip zone have similar sterane concentrations but higher sterane 20S values in the MS (i.e., sample 8), it should be interpreted as an enrichment in steranes in the MS, since the rock volume used to calculate yields for MS and SZ is the same (see sections 3.3.2 and 4.1). Moreover, an enrichment in biomarkers concentration is observed in the slip zones of some natural samples, with respect to the associated control samples (i.e., samples 6B, 9A, 7B; Figure 4c, d, e, f), and in the slip zone of the shear-experimental sample obtained at 3 m/s, if compared to the other experimental slip zones (Figure 5c, d, e, f). In contrast, MS for the same samples, usually show 1-2 orders of magnitude decrease in overall sterane concentrations, which does not coincide with an increase of the sterane 20S parameter. This can be compared to the static-heating experiments, where bituminous dolostone powders heated for 2-10 seconds present lower concentrations of sterane, and little change in the 20S sterane parameter (Figure 4). Thus, when isomers are generated in the slip zone and then disappear in the MS, the increase of the sterane 20S parameter suggests a similar behavior to the shortest duration static-heating experiments. This also implies that, in most cases, steranes from rotary-shear experiments were mildly altered or not thermally altered at all. Similar to the steranes, the highest concentrations of hopanes were found in slip zones, sometimes exceeding that of the control samples, both in shear- and static-heating experimental samples. This is consistent with the generation of new hopanes via the thermal breakdown of geomacromolecules (e.g., asphaltic material within the protobitumen). This is important as models of changes in biomarker thermal maturity parameters depend on differences in relative rates of both thermal degradation, and generation of new isomers from cracking of larger macromolecules (Bishop and Abbot, 1995; Farrimond et al., 1998). Much reduced generation of steranes and hopane isomers from geomacromolecules, evidenced by concentrations that do not exceed starting or control values, has implications for how the sterane 20S and hopane 22S parameter may function in frictional heating as compared to burial diagenesis (Figure 6).

Microstructural investigations of the natural sampled faults show that (i) multiple slip events were recorded in faults with at least 0.12 m of slip, and that slip zones bounded by a MS experienced embrittlement and fragmentation possibly associated with seismic slip, but also pressure-solution of dolomite and viscous flow of bitumen during the seismic cycle (Chinello et al., 2023). As a consequence, displacement accommodated by these faults can result from (i) a single seismic event, (ii) aseismic (creep) events at slip rates of nm-µm/s or less, (iii) a combination of both, but also from (iv) multiple seismic and aseismic slip events. These four options can explain why there is poor correlation between the thermal maturity/concentration values and the total displacement accommodated by the faults. However, the probability of having experienced at least one seismic event is higher in faults with the highest displacement, and the thermal maturity values of the MSs and higher isomers concentration (see discussion above) seem to correlate better (Figures 4g, 5g). It is also possible that the activation of coseismic processes like mechanical and thermal fluid pressurization, which should not result in large temperature increase in the slip zone (Rice, 2006; Aretusini et al., 2021a), may prevent an increase in thermal maturity. In addition, during the seismic cycle, deformation in fault cores may localize in a principal slip zone where most strain deformation is accommodated, or over a number of secondary fault/fractures that may cut the control part of the samples analyzed resulting in very local to broad variations of thermal maturity.

The heterogeneous distribution of frictional heating on the same fault, due for instance to surface roughness, stress or seismic slip rate distribution (Figure 7), may control the response of the biomarkers thermal maturity parameters (see the different thermal maturity trends observed between parts “A” and “B” in Figures 4, 5). Processes like flash heating can increase the temperature at the asperity scale (10-100 μm) up to ≈1000 °C in milliseconds (Rice, 2006; Spagnuolo et al. 2015). Flash-heating of protobitumen can generate isomers in a similar way to the thermally induced breakdown of asphaltene and kerogen during flash pyrolysis (Philp and Gilbert, 1985). Then, because of fault roughness, the stress normal to the fault can be much higher than the one applied in the experiments (20 MPa), also at 1-3 km depth (e.g., Griffith et al., 2010). In addition, co-seismic slip rates could be higher than 1-3 m/s, especially near the tip of the propagating seismic rupture (e.g., Harbord et al., 2021). Since the bulk temperature increase during frictional sliding is proportional to slip distance, normal stress and slip rate (Carslaw and Jaeger, 1959), in some natural cm-m long fault patches the temperature increase could be well above the ≈350 °C measured in our experiments and therefore thermal maturation larger. Heating exposures of 1 and 5 minutes investigated in the static-heating experiments are not compatible with the typical rise time (or short duration of slip pulses lasting <<1s) of small in magnitude earthquakes (Mw <4), but the temperature recorded by the thermocouple (≈350 °C) underestimates the “real” temperatures (see discussion in Aretusini et al. (2021b). For these reasons, the high thermal maturity measured (i) in some of the natural MSs (samples 8A-B, 2B and 9B), (ii) in MSs obtained in rotary-shear experiments performed at seismic slip rates, together with (iii) the increase in thermal maturity of bituminous dolostones after 1-5 minutes of heating during the static-heating experiments (Figures 4, 5), are still compatible with frictional heating during earthquakes. However, a kinetic model of steranes and hopanes in extractable organic matter (i.e., bitumen) is necessary to understand better the time-temperature evolution of these biomarkers and the energy necessary to activate the maturation process. Such a model should also include mechano-chemical effects, typical of grain size reduction and amorphization processes associated with frictional sliding, which may lower the activation energy and may alter the kinetics of the reactions involved in the thermal maturation of biomarkers.

5.4 Molecular marker parameters applied in similar contexts

Thermal maturity in fault zones has been investigated using molecular markers such as methylphenanthrenes, diamondoids, n-alkanes, alkenones, and the Carbon Preference Index (Savage et al., 2014; Savage et al., 2018; Savage and Polissar, 2019; Coffey et al., 2019; Rabinowitz et al., 2020). However, this is the first study to report on the sterane 20S and hopane 22S parameters in this context. Differences in the rates of change of biomarker thermal maturity parameters across rifted basins were previously documented by McKenzie and Mackenzie (1983), although those comparisons primarily focused on aromatization and isomerization reactions. Since then, it has become clear that the "isomerization" reflected in sterane 20S and hopane 22S ratios does not represent a simple parent–child transformation (intra-conversion). For example, the sterane 20S isomer does not arise solely from direct conversion of the 20R isomer; instead, both 20S and 20R isomers are destroyed at different rates, and additional 20S and 20R isomers are generated through the release of covalently bound counterparts from kerogen (Bishop and Abbott, 1993; Farrimond et al., 1998). Consequently, the distinct trends observed for burial heating versus frictional heating (Figure 6) may reflect differences in rates of generation, destruction and intra-conversion.

Studies of natural samples have shown that a range of biomarkers record increases in thermal maturity in fault zones that experienced seismic slip and temperatures sufficient to form pseudotachylytes (Savage et al., 2014). Experimental work further demonstrated that the MPI-4 parameter increases after ≈10 m of slip at rates that generate temperatures ≥ 500 °C (Savage et al., 2018). Taken together, the hopane 22S and sterane 20S parameters presented here appear particularly well suited for detecting heating associated with seismic slip in faults with total displacements of ≈0.5–10 m, especially where the host rock is rich in organic carbon, contains pre–oil window organic matter, and experiences relatively moderate peak temperatures (e.g., ≈400 °C). However, the concurrent destruction and generation of isomers observed in static-heating experiments at maturity levels comparable to all but one of the natural samples indicates that additional high-temperature studies on fault rocks are needed to fully constrain the behavior of sterane and hopane maturity parameters during frictional heating associated with seismic slip.

6 Conclusions

In this study we investigate thermal maturity changes associated with frictional heating pulses during seismic slip in fault rocks bounded by Mirror-like Surfaces (MSs) in bituminous dolostones. To measure thermal maturity in fault zones at the sample scale (Figure 3) we used the 20S and hopane 22S biomarkers parameters, commonly used to investigate the thermal maturity of shallow sedimentary basin rocks (Figure 1). We measured the thermal maturity of the host rock (*Dolomie Bituminose* Fm., Monte Camicia Thrust area, Italian Central Apennines; Figure 2) as well as of MSs and their associated slip zone along natural faults with displacements ranging from a few millimeters to a few meters. The biomarkers response of natural samples was calibrated by analyzing rock powders subjected to static-heating experiments performed at 400 °C with exposure times ranging from 2 seconds to 12 hours, and by analyzing artificial MSs produced in experiments at sub-seismic (0.0001 m/s) and seismic (1-3 m/s) slip rates (Figure 2). Our results indicate that:

(i) the MSs of some natural samples exhibit higher thermal maturity compared to the associated slip zone and/or control part (Figures 4a, c, 5b),

(ii) an increase in thermal maturity occurs after 1-5 minutes of static exposure at 400 °C together with an increase in the concentrations of steranes and hopanes after at least 30 s of heating,

(iii) experimental MSs produced at seismic slip rates have higher thermal maturity than the associated slip zone (Figures 4b, d, 5a), and

(iv) both experimental and natural MSs with higher thermal maturity relative to the associated slip zone follow a maturity trend that differs from the “classic” burial trend observed in sedimentary basins and reproduced by the static-heating experiments, showing higher sterane 20S values for an equivalent hopane 22S parameter (Figure 6).

Temperatures in natural seismic slip zones, including those at the studied outcrop, can be significantly higher than those examined in the experiments, and thermal maturation rates much faster at higher temperatures. We conclude that thermal maturity investigations based on sterane and hopane biomarkers can detect increases in temperature related to frictional heating pulses during earthquakes, and the seismic origin of some MSs. This approach may allow us to distinguish MSs produced during seismic faulting from those produced at aseismic deformation conditions. This is useful also for seismic hazard purposes to distinguish seismic from creeping active faults.

Acknowledgments

This research was founded by a INGV PhD grant: “Formation of polished surfaces in natural rocks: experimental and field constraints” (MC), by the project PRIN 2022WE2JY9 SCHOTTA (GDT and MC), by the project ERC 614705 NOFEAR (GDT and MC), and the project MUR-Dipartimenti di Eccellenza 2023–2027 C93C23002690001 Geosciences (GDT and TT). AS acknowledges the public fundings of the Ramón y Cajal Program (RYC-2022) nº RYC2022-036094-I MCIN/AEI/10.13039501100011033, funded by the Spanish Ministry of Science and Innovation and cofounded by the European Union (FSE+). The authors thank Alessio Pontesilli and Chiara Dalconi for helping during the static-heating experiments and Michele Fondriest and Chiara Cornelio for the constructive discussions.

Open Research

All the data are publicly available online (Chinello et al., 2026).

Conflict of Interest Disclosure

The authors declare there are no conflicts of interest in this manuscript.

References

Adamoli, L., Mancinelli, A., Pieruccini, U., and Romano, A. (1984). Ricerche Geologiche Sul Gran Sasso d'Italia (Abruzzo). VIII. Età e Significato Paleoambientale Degli 'Scisti Bituminosi'. *Studi Geologici Camerti*, *IX*, 7–14.

Adamoli, L., Bigozzi, A., Ciarapica, G., Cirilli, S., Passeri, L., Romano, A., Duranti, F. and Venturi, F. (1990). Upper Triassic Bituminous Facies and Hettangian Pelagic Facies in the Gran Sasso Range. *Bollettino Della Società Geologica Italiana* 109: 219–30.

Agosta, F., Dastoli, S.M., Taddeo, C.E., Abdallah, I.B., Curzi, M., Mercuri, M. and Corradetti, A. (2026). Geometry, kinematics, and roughness properties of segmented normal fault zones: insights from the Monte Capo di Serre carbonate fault zone, central Italy. *Journal of Structural Geology* 207, 105673. https://doi.org/10.1016/j.jsg.2026.105673.

Alkhafaji, M.W., Connan, J., Engel, M.H. and Al-Jubouri, S.W. (2021). Origin, biodegradation, and water washing of bitumen from the Mishraq Sulfur Mine, northern Iraq. *Marine and Petroleum Geology* 124, 104786.

Aretusini, S., Meneghini, F., Spagnuolo, E., Harbord, C. W., and Di Toro, G., (2021a). Fluid Pressurisation and Earthquake Propagation in the Hikurangi Subduction Zone. *Nature Communications* 12 (1). https://doi.org/10.1038/s41467-021-22805-w.

Aretusini, S., Núñez-Cascajero, A., Spagnuolo, E., Tapetado, A., Vázquez, C. and Di Toro, G. (2021b). Fast and Localized Temperature Measurements During Simulated Earthquakes in Carbonate Rocks. *Geophysical Research Letters* 48 (9). https://doi.org/10.1029/2020GL091856.

Aubry, J., Passelègue, F. X., Escartín, J., Gasc, J., Deldicque, D., and Schubnel, A. (2020). Fault stability across the seismogenic zone. *Journal of Geophysical Research: Solid Earth*, 125, e2020JB019670. https://doi.org/10.1029/2020JB019670.

Barchi, M. and Bigozzi, A. (1995). Ipotesi Sulla Geometria e La Genesi Dei Bacini Euxinici Del Trias Superiore in Appennino Centrale. *Studi Geologici Camerti, Speciale*, *1*, 53–62.

Bertinelli, A., Nannarone, C., Passeri, L. and Venturi, F. (2004). Hettangian Ammonites and Radiolarians in the Mt. Camicia (Gran Sasso, Central Apennines). *Rivista Italiana Di Paleontologia e Stratigrafia* 110 (1): 87–95. https://doi.org/10.13130/2039-4942/6270.

Bishop, A.N. and Abbott, G.D. (1993). The interrelationship of biological marker maturity parameters and molecular yields during contact metamorphism, *Geochimica et Cosmochimica Acta* 57, 15, 3661-3668. https://doi.org/10.1016/0016-7037(93)90147-O.

Bishop, A.N. and Abbott, G.D. (1995). Vitrinite reflectance and molecular geochemistry of Jurassic sediments: the influence of heating by Tertiary dykes (northwest Scotland). *Organic Geochemistry* 22, 1, 165-177, https://doi.org/10.1016/0146-6380(95)90015-2.

Boneh, Y., Sagy, A. and Reches, Z. (2013). Frictional Strength and Wear-Rate of Carbonate Faults during High-Velocity, Steady-State Sliding. *Earth and Planetary Science Letters* 381: 127–37. https://doi.org/10.1016/j.epsl.2013.08.050.

Bowden, F. P., and Tabor, D. (1950). The Friction and Lubrication of Solids. *Oxford: Clarendon Press*.

Bowden, S. A., Farrimond, P., Snape, C. E. and Love, G. D. (2006). Compositional differences in biomarker constituents of the hydrocarbon, resin, asphaltene and kerogen fractions: An example from the Jet Rock (Yorkshire, UK), *Organic Geo-chemistry*, 37, 369–383, https://doi.org/10.1016/j.orggeochem.2005.08.024.

Buseck, P. R. and Beyssac, O. (2014). From Organic Matter to Graphite: Graphitization. *Elements* 10 (6): 421–26. https://doi.org/10.2113/gselements.10.6.421.

Bustin, R. M. (1983). Heating during thrust faulting in the Rocky Mountains: Friction or fiction, *Tectonophysics*, 95, 309–328.

Calzolari, G., Ault, A. K., Hirth, G. and McDermott, R. G. (2020). Hematite (U-Th)/He Thermochronometry Detects Asperity Flash Heating during Laboratory Earthquakes. *Geology* 48 (5): 514–18. https://doi.org/10.1130/G46965.1.

Carslaw, H.S. and Jaeger, J.C. (1959). Conduction of Heat in Solids, 2nd edition. Oxford at the Clarendon Press, Oxford.

Cazzini, F., Zotto, O.D., Fantoni, R., Ghielmi, M., Ronchi, P. and Scotti, P. (2015). Oil and gas in the Adriatic foreland, Italy. J. Petrol. Geol. 38 (3), 255–279.

Chinello, M., Bersan, E., Fondriest, M., Tesei, T., Gomila, R. and Di Toro, G. (2023). Seismic Cycle in Bituminous Dolostones (Monte Camicia Thrust Zone, Central Apennines, Italy). *Geochemistry, Geophysics, Geosystems* 24 (12). https://doi.org/10.1029/2023GC011063.

Chinello, M., Aretusini S., Spagnuolo, E., Nava, J., Tesei, T., Fondriest, M. and Di Toro, G. (under review). Seismic vs. sub-seismic Experimental Mirror-like Fault Surfaces in Bituminous Dolostones, *Journal of Geophysical Research: Solid Earth*.

Chinello, M., Schito, A., Bowden, S. A., Spagnuolo, E., Aretusini, S., Tesei, T., and Di Toro, G. (2026). Biomarkers Thermal Maturity Parameters in Bitumen as a Proxy for Seismic vs. Aseismic Mirror-like Fault Surfaces. [Dataset]. Research Data Unipd. https://researchdata.cab.unipd.it/id/eprint/1891

Coffey, G. L., Savage, H. M., Polissar, P. J., Rowe, C. D. and Rabinowitz, H. S., (2019). Hot on the trail: Coseismic heating on a localized structure along the Muddy Mountain fault, Nevada. *Journal of Structural Geology* 120,67–79.

Cornelio, C., Aretusini, S., Spagnuolo, E., Di Toro, G. and Cocco, M. (2024). Multiple Seismic Slip-Rate Pulses and Mechanical and Textural Evolution of Calcite-Bearing Fault Gouges. *Journal of Geophysical Research: Solid Earth* 129 (7). https://doi.org/10.1029/2024JB029099.

Cortinovis, S., Fondriest, M., Balsamo, F., Lucca, A., La Valle, F., Pizzati, M., Storti, F. and Di Toro, G. (2024). In-Situ Rock Shattering and Strain Localization along a Seismogenic Fault in Dolostones (Monte Marine Fault, Italian Central Apennines). *Journal of Structural Geology* 183 (April): 105144. https://doi.org/10.1016/j.jsg.2024.105144.

Curiale, J. A. (1986). Origin of Solid Bitumens, with Emphasis on Biological Marker Results. *Organic Geochemistry* 10 (1–3): 559–80. https://doi.org/10.1016/0146-6380(86)90054-9.

Curzi, M., Billi, A., Aldega, L., Baneschi, I., Boschi, C., Caracausi, A., Cavallo, A., Ruggieri G. and Carminati E. (2026). *Nature Communications* **17**, 2766 https://doi.org/10.1038/s41467-026-69174-w.

De Paola, N., Hirose, T., Mitchell, T., Di Toro, G., Viti, C. and Shimamoto, T. (2011). Fault Lubrication and Earthquake Propagation in Thermally Unstable Rocks. *Geology* 39 (1): 35–38. https://doi.org/10.1130/G31398.1.

De Paola, N., Holdsworth, R. E., Viti, C., Collettini, C. and Bullock, R. (2015). Can Grain Size Sensitive Flow Lubricate Faults during the Initial Stages of Earthquake Propagation? *Earth and Planetary Science Letters* 431: 48–58. https://doi.org/10.1016/j.epsl.2015.09.002.

Demurtas, M., Fondriest, M., Balsamo, F., Clemenzi, L., Storti, F., Bistacchi, A. and Di Toro, G. (2016). Structure of a Normal Seismogenic Fault Zone in Carbonates: The Vado Di Corno Fault, Campo Imperatore, Central Apennines (Italy). *Journal of Structural Geology* 90: 185–206. https://doi.org/10.1016/j.jsg.2016.08.004.

Demurtas, M., Smith, S. A.F., Spagnuolo, E. and Di Toro, G. (2021). Frictional Properties and Microstructural Evolution of Dry and Wet Calcite–Dolomite Gouges. *Solid Earth* 12 (3): 595–612. https://doi.org/10.5194/se-12-595-2021.

Di Toro, G., Niemeijer, A., Tripoli, A., Nielsen, S., Di Felice, F., Scarlato, P., Spada, G., Alessandroni, R., Romeo, G., Di Stefano, G., Smith, S.A.F., Spagnuolo, E. and Mariano, S. (2010). From Field Geology to Earthquake Simulation: A New State-of-The-Art Tool to Investigate Rock Friction during the Seismic Cycle (SHIVA). *Rendiconti Lincei* 21 (SUPPL. 1): 95–114.

Fan, C., Liu, J., Hunfeld, L. B. and Spiers, C. J. (2020). Frictional Slip Weakening and Shear-Enhanced Crystallinity in Simulated Coal Fault Gouges at Slow Slip Rates. *Solid Earth* 11 (4): 1399–1422. https://doi.org/10.5194/se-11-1399-2020.

Farrimond, P., Taylor, A. and TelnÆs, N. (1998). Biomarker Maturity Parameters: The Role of Generation and Thermal Degradation. *Organic Geochemistry* 29 (5-7–7 pt 2): 1181–97. https://doi.org/10.1016/S0146-6380(98)00079-5.

733 Felinger, A. (2011). Estimation of chromatographic peak shape parameters in Fourier domain. *Talanta*. Jan 30;83(4):1074-8. doi: 10.1016/j.talanta.2010.10.001. Epub 2010 Oct 8. PMID: 21215841.

735 Fondriest, M., Smith, S. A. F., Di Toro, G., Zampieri, D. and Mittempergher, S. (2012). Fault Zone Structure and Seismic Slip Localization in Dolostones, an Example from the Southern Alps, Italy. *Journal of Structural Geology* 45: 52–67. https://doi.org/10.1016/j.jsg.2012.06.014.

738 Fondriest, M., Smith, S. A. F., Candela, T., Nielsen, S. B., Mair, K. and Di Toro, G. (2013). Mirror-like Faults and Power Dissipation during Earthquakes. *Geology* 41 (11): 1175–78. https://doi.org/10.1130/G34641.1.

740 Fondriest, M., Aretusini, S., Di Toro, G. and Smith, S. A. F. (2015). Fracturing and Rock Pulverization along an Exhumed Seismogenic Fault Zone in Dolostones: The Foiana Fault Zone (Southern Alps, Italy). *Tectonophysics* 654: 56–74. https://doi.org/10.1016/j.tecto.2015.04.015.

743 Furuichi, H., Ujiie, K., Kouketsu, Y., Saito, T., Tsutsumi, A. and Wallis, S. (2015). Vitrinite Reflectance and Raman Spectra of Carbonaceous Material as Indicators of Frictional Heating on Faults: Constraints from Friction Experiments. *Earth and Planetary Science Letters* 424: 191–200. https://doi.org/10.1016/j.epsl.2015.05.037.

747 Ghisetti, F., and Vezzani, L. (1986). Assetto Geometrico Ed Evoluzione Strutturale Della Catena Del Gran Sasso Tra Vado Di Siella e Vado Di Corno. *Bollettino della Societa Geologica Italiana e del Servizio Geologico d'Italia*, *105*, 131–171.

750 Ghisetti, F. (1987). Mechanisms of thrust faulting in the Gran Sasso Chain, Central Apennines, Italy. *Journal of Structural Geology*, *9*(8), 955–967. https://doi.org/10.1016/0191-8141(87)90004-6.

752 Ghisetti, F., and Vezzani, L. (1991). Thrust belt development in the Central Apennines (Italy): Northward polarity of thrusting and out-of-Sequence deformations in the Gran Sasso Chain. *Tectonics*, 10(5), 904–919. https://doi.org/10.1038/s41407-022-0858-2.

755 Griffith, W. A., Nielsen, S., Di Toro, G. and Smith, S. A. (2010), Rough faults, distributed weakening, and off-fault deformation, *Journal of Geophysical Research: Solid Earth*, 115, B08409, doi:10.1029/2009JB006925.

758 Han, R., Shimamoto, T., Hirose, T., Ree, J.-H., and Ando, J.-I. (2007). Ultralow friction of carbonate faults caused by thermal decomposition. *Science*, 316(5826), 878–881. https://doi.org/10.1126/science.1139763.

761 Han, R., Hirose, T. and Shimamoto, T. (2010), Strong velocity weakening and powder lubrication of simulated carbonate faults at seismic slip rates, *Journal of Geophysical Research*, 115, B03412, doi:10.1029/2008JB006136.

764 Hancock, P.L. and Barka, A.A., (1987). Kinematic indicators on active nor- mal faults in western Turkey. *Journal of Structural Geology* 9, 419± 427.

766 Harbord, C., Brantut, N., Spagnuolo, E. and Di Toro, G. (2021). Fault friction during simulated seismic slip pulses. *Journal of Geophysical Research: Solid Earth*, 126, e2021JB022149.

768 Henry, D. G., Jarvis, I., Gillmore, G. and Stephenson, M. (2019). Raman Spectroscopy as a Tool to Determine the Thermal Maturity of Organic Matter: Application to Sedimentary, Metamorphic and Structural Geology. *Earth-Science Reviews* 198 (June): 102936. https://doi.org/10.1016/j.earscirev.2019.102936.

771 Hirono, T., Maekawa, Y. and Yabuta H. (2015). Investigation of the records of earthquake slip in carbonaceous materials from the Taiwan Chelungpu fault by means of infrared and Raman spectroscopies, *Geochemistry, Geophysics, Geosystems*, 16, 1233–1253, doi:10.1002/ 2014GC005622.

774 Ito, K., Ujiie, K. and Kagi, H. (2017). Detection of Increased Heating and Estimation of Coseismic Shear Stress from Raman Spectra of Carbonaceous Material in Pseudotachylytes. *Geophysical Research Letters* 44 (4): 1749–57. https://doi.org/10.1002/2016GL072457.

777 Jackson, J., and McKenzie, D. (1999). A Hectare of Fresh Striations on the Arkitsa Fault, Central Greece. *Journal of Structural Geology* 21 (1): 1–6. https://doi.org/10.1016/S0191-8141(98)00091-1.

779 Kaneki, S., Hirono, T., Mukoyoshi, H., Sampei, Y. and Ikehara, M. (2016). Organochemical characteristics of carbonaceous materials as indicators of heat recorded on an ancient plate-subduction fault. *Geochemistry, Geophysics, Geosystems* 17, 2855–2868, doi:10.1002/2016GC006368.

782 Kaneki, S., Ichiba, T. and Hirono, T. (2018). Mechanochemical Effect on Maturation of Carbonaceous Material:

Implications for Thermal Maturity as a Proxy for Temperature in Estimation of Coseismic Slip Parameters. *Geophysical Research Letters* 45 (5): 2248–56. https://doi.org/10.1002/2017GL076791.

Katz, B. J., Dittmar, E. I. and Ehret, G. E. (2000). A geochemical review of carbonate source rocks in Italy. *Journal of Petroleum Geology*, 23(4), 399–424. https://doi.org/10.1111/j.1747-5457.2000.tb00494.x.

Kedar, L., Bond, C. E. and Muirhead, D. (2020). Carbon ordering in an aseismic shear zone: Implications for Raman geothermometry and strain tracking. *Earth and Planetary Science Letters*, 549, 116536.

Kitamura, M., Mukoyoshi, H., Fulton, p. M. and Hirose, T. (2012). Coal Maturation by Frictional Heat during Rapid Fault Slip. *Geophysical Research Letters* 39 (16): 1–3. https://doi.org/10.1029/2012GL052316.

Kolaczkowska, E., Slougui, N.-E., Watt, D. S., Maruca, R. E. and Moldowan, J. M. (1990) Thermodynamic stability of various alkylated, dealkylated and re- arranged 17a- and 17b-hopane isomers using molecular mechanics calculations. *Organic Geochemistry* 16, 1033± 1038.

Koppensteiner, S. J., Bauer, H., Grasemann, B., Plan, L. and Baroň, I. (2025). Fault mirrors in the process zone of a seismogenic fault (Karawanks, Eastern Alps). *Austrian Journal of Earth Sciences*, 118(1), 115-132.

Kuo, L. W., Di Felice, F., Spagnuolo, E., Di Toro, G., Rong Song, C., Aretusini, S., Li, H., Suppe, J., Si, J. and Wen, C.-Y. (2017). Fault Gouge Graphitization as Evidence of Past Seismic Slip. *Geology* 45 (11): 979–82. https://doi.org/10.1130/G39295.1.

Leah, H., Fondriest, M., Lucca, A., Storti, F., Balsamo, F. and Di Toro, G. (2018). Coseismic Extension Recorded within the Damage Zone of the Vado Di Ferruccio Thrust Fault, Central Apennines, Italy. *Journal of Structural Geology* 114 (March): 121–38. https://doi.org/10.1016/j.jsg.2018.06.015.

Lipparini, L., D'Ambrosio, A., Trippetta, F., Bigi, S., Derks, J. F., Bambridge, V. R. And Cassola, T. (2021). A new regional petroleum systems model for Central Italy and the central Adriatic Sea supported by basin modelling and an analysis of hydrocarbon occurrences. *Journal of Petroleum Geology*, *44*(4), 461-485.

Lucca, A., Storti, F., Balsamo, F., Clemenzi, L., Fondriest, M., Burgess, R., and Di Toro, G. (2019). From submarine to subaerial out-of-sequence thrusting and Gravity-driven extensional faulting: Gran Sasso massif, Central Apennines, Italy. *Tectonics*, *38*(12), 4155–4184. https://doi.org/10.1029/2019TC005783.

Mackenzie, A. S., Patience, R. L., Maxwell, J. R., Vandenbroucke, M. and Durand, B. (1980). Molecular parameters of maturation in the Toarcian shales, Paris Basin, France-I. Changes in the configurations of acyclic isoprenoid alkanes, steranes and triterpanes. *Geochimica et Cosmochimica Acta* 44, 1709±1721.

Mackenzie, A. S., and McKenzie, D. (1983). Isomerization and Aromatization of Hydrocarbons in Sedimentary Basins Formed by Extension. *Geological Magazine* 120 (5): 417–70. https://doi.org/10.1017/S0016756800027461.

Mastalerz, M., Brobniak, A. and Stankiewicz, A.B. (2018). Origin, properties, and implications of solid bitumen in source-rock reservoirs: a review. *International Journal of Coal Geology* 195, 14–36.

Mastalerz, M., Wilks, K. R., Bustin, R. M. and Ross, J. V. (1993). The Effect of Temperature, Pressure and Strain on Carbonization in High-Volatile Bituminous and Anthracitic Coals. *Organic Geochemistry* 20 (2): 315–25. https://doi.org/10.1016/0146-6380(93)90047-F.

McDermott, R.G., Ault, A.K., Evans, J.P., and Reiners, P.W. (2017). Thermochronometric and textural evidence for seismicity via asperity flash heating on exhumed hematite fault mirrors, Wasatch fault zone, UT, USA. *Earth and Planetary Science Letters*, v. 471, p. 85–93, https://doi.org/10.1016/j.epsl.2017.04.020.

Morozov, Yu A., Bukalov, S. S. and Leites, L. A. (2020). Structural Transformations of Sp2 Carbon in the Zones of Seismogenic Faults in Carbonate and Silicate Rocks. *Doklady Earth Sciences* 490 (2): 60–64. https://doi.org/10.1134/S1028334X20020099.

Muirhead, D. K., Kedar, L. , Schito, A., Corrado, S., Bond, C. E. and Romano, C. (2021). Raman Spectral Shifts in Naturally Faulted Rocks. *Geochemistry, Geophysics, Geosystems* 22 (10): 1–13. https://doi.org/10.1029/2021gc009923.

Nielsen, S. B., Spagnuolo, E., Violay, M. and Di Toro, G. (2021). Thermal weakening friction during seismic slip: Experiments and models with heat sources and sinks. *Journal of Geophysical Research: Solid Earth*, 126(5), e2020JB020652. https://doi.org/10.1029/2020JB020652.

Niemeijer, A., Di Toro, G., Griffith, W. A., Bistacchi, A., Smith, S. A.F. and Nielsen, S. (2012). Inferring earthquake physics and chemistry using an integrated field and laboratory approach, *Journal of*

Structural Geology, 39, 2-36. https://doi.org/10.1016/j.jsg.2012.02.018.

O'Hara, K. (2004). Paleo-Stress Estimates on Ancient Seismogenic Faults Based on Frictional Heating of Coal. *Geophysical Research Letters* 31 (3): 2–5. https://doi.org/10.1029/2003GL018890.

O'Hara, K., Mizoguchi, K., Shimamoto, T. and Hower, J. C. (2006). Experimental Frictional Heating of Coal Gouge at Seismic Slip Rates: Evidence for Devolatilization and Thermal Pressurization of Gouge Fluids. *Tectonophysics* 424 (1–2): 109–18. https://doi.org/10.1016/j.tecto.2006.07.007.

Ohl, M., Plümper, O., Chatzaras, V., Wallis, D., Vollmer, C. and Drury, M. (2020). Mechanisms of Fault Mirror Formation and Fault Healing in Carbonate Rocks. *Earth and Planetary Science Letters* 530: 115886. https://doi.org/10.1016/j.epsl.2019.115886.

Park, Y., Hirose, T. and Ree, J. H. (2021). Carbonate Fault Mirrors With Extremely Low Frictional Healing Rates: A Possible Source of Aseismic Creep. *Geophysical Research Letters* 48 (11). https://doi.org/10.1029/2021GL093749.

Passelègue, F. X., Aubry, J., Nicolas, A., Fondriest, M., Deldicque, D., Schubnel, A. and Di Toro, G. (2019). From Fault Creep to Slow and Fast Earthquakes in Carbonates. *Geology* 47 (8): 744–48. https://doi.org/10.1130/G45868.1.

Peters, K.E., Walters, C.C. and Moldowan, J.M. (2005). The Biomarker Guide. In: Vol. 2: Biomarkers and Isotopes in Petroleum Exploration and Earth History. Second ed. *Cambridge University Press*.

Peters, K.E., Moldowan, J.M. (2017). Biomarkers: Assessment of Source Rock Thermal Maturity. In: Sorkhabi, R. (eds) Encyclopedia of Petroleum Geoscience. Encyclopedia of Earth Sciences Series. *Springer*. https://doi.org/10.1007/978-3-319-02330-4_10-1

Philp, R.P. and Gilbert, T.D. (1985). Source rock and asphaltene biomarker characterization by pyrolysis-gas chromatography-mass spectrometry-multiple ion detection. *Geochimica et Cosmochimica Acta*, 49, 6. https://doi.org/10.1016/0016-7037(85)90292-3.

Polissar, P. J., Savage, H. M. and Brodsky, E. E. (2011). Extractable Organic Material in Fault Zones as a Tool to Investigate Frictional Stress. *Earth and Planetary Science Letters* 311 (3–4): 439–47. https://doi.org/10.1016/j.epsl.2011.09.004.

Pozzi, G., De Paola, N., Nielsen, S. B., Holdsworth, R. E. and Bowen, L. (2018). A New Interpretation for the Nature and Significance of Mirror-like Surfaces in Experimental Carbonate-Hosted Seismic Faults. *Geology* 46 (7): 583–86. https://doi.org/10.1130/G40197.1.

Pozzi, G., De Paola, N., Holdsworth, R. E., Bowen, L., Nielsen, S. B. and Dempsey, E. D. (2019). Coseismic Ultramylonites: An Investigation of Nanoscale Viscous Flow and Fault Weakening during Seismic Slip. *Earth and Planetary Science Letters* 516: 164–75. https://doi.org/10.1016/j.epsl.2019.03.042.

Rabinowitz, H., Polissar, P. and Savage, H. (2017). Reaction kinetics of alkenone and n-alkane thermal alteration at seismic timescales. *Geochemistry, Geophysics, Geosystems*, 18(1), 204–219. https://doi.org/10.1002/2016gc006553.

Rabinowitz, H. S., Savage, H. M., Polissar, P. J., Rowe, C. D. and Kirkpatrick, J.D. (2020). Earthquake Slip Surfaces Identified by Biomarker Thermal Maturity within the 2011 Tohoku-Oki Earthquake Fault Zone. *Nature Communications* 11 (1): 1–9. https://doi.org/10.1038/s41467-020-14447-1.

Radke, M. and Welte, D. H. (1983). The Methylphenanthrene Index (MPI): a maturity parameter based on aromatic hydrocarbons. In Advances in Organic Geochemistry 1981 (Edited by Bjoroy M. et al.), pp. 504-512. Wiley, Chichester.

Radke, M., (1988). Application of aromatic compounds as maturity indicators in source rocks and crude oils. Marine and Petroleum Geology, Volume 5, Issue 3. https://doi.org/10.1016/0264-8172(88)90003-7.

Rempe, M., Di Toro, G., Mitchell, T. M., Smith, S. A. F., Hirose, T. and Renner, J. (2020). Influence of effective stress and pore fluid pressure on fault strength and slip localization in carbonate slip zones. *Journal of Geophysical Research: Solid Earth*, 125, e2020JB019805. https://doi.org/10.1029/2020JB019805.

Rice, J. R. (2006). Heating and Weakening of Faults during Earthquake Slip. *Journal of Geophysical Research: Solid Earth* 111 (5): 1–29. https://doi.org/10.1029/2005JB004006.

Rowe, C. D. and Griffith, W. A. (2015). Do Faults Preserve a Record of Seismic Slip: A Second Opinion. *Journal of Structural Geology* 78: 1–26. https://doi.org/10.1016/j.jsg.2015.06.006.

Rusciadelli, G., Viandante, M. G., Calamita, F. and Cook, A. C. (2005). Burial-exhumation history of the Central Apennines (Italy), from the Foreland to the Chain Building: Thermochronological and Geological data. *Terra Nova*, *17*(6), 560–572. https://doi.org/10.1111/j.1365-3121.2005.00649.x

Sanei, H. (2020). Genesis of solid bitumen. *Scientific Reports*, 10, 15595. https://doi.org/10.1038/s41598-020-72692-2.

Sakaguchi, A., Chester, F., Curewitz, D., Fabbri, O., Goldsby, D., Kimura, G., Li, C.-F., Masaki, Y., Screaton, E. J., Tsutsumi, A., Ujiie, K. and Yamaguchi, A. (2011). Seismic slip propagation to the updip end of plate boundary subduction interface faults: Vitrinite reflectance geothermometry on Integrated Ocean Drilling Program NanTro SEIZE cores. *Geology*; 39 (4): 395–398. https://doi.org/10.1130/G31642.1.

Savage, H. M., Polissar, P. J., Sheppard, R., Rowe, C. D. and Brodsky, E. E. (2014). Biomarkers Heat up during Earthquakes: New Evidence of Seismic Slip in the Rock Record. *Geology* 42 (2): 99–102. https://doi.org/10.1130/G34901.1.

Savage, H. M., Rabinowitz, H. S., Spagnuolo, E., Aretusini, S., Polissar, P. J. and Di Toro, G. (2018). Biomarker Thermal Maturity Experiments at Earthquake Slip Rates. *Earth and Planetary Science Letters* 502: 253–61. https://doi.org/10.1016/j.epsl.2018.08.038.

Savage, H. M. and Polissar, P. J. (2019). Biomarker Thermal Maturity Reveals Localized Temperature Rise From Paleoseismic Slip Along the Punchbowl Fault, CA, USA. *Geochemistry, Geophysics, Geosystems* 20 (7): 3201–15. https://doi.org/10.1029/2019GC008225.

Schito, A., Pensa, A., Romano, C., Corrado, S., Vona, A., Trolese, M., Morgavi, D. and Giordano, G. (2022). Calibrating carbonization temperatures of wood fragments embedded within pyroclastic density currents through Raman spectroscopy. *Minerals* 12 (2), 203. https://doi.org/10.3390/min12020203.

Schito, A., Muirhead, D.K., Parnell, J. (2023). Towards a kerogen-to-graphite kinetic model by means of Raman spectroscopy, *Earth-Science Reviews*, 237, 104292, https://doi.org/10.1016/j.earscirev.2022.104292.

Scholz, C. (2019). The mechanics of earthquakes and faulting (3rd ed.). *Cambridge University Press*.

Sheppard, R. E., Polissar, P. J. and Savage, H, M. (2015). Organic Thermal Maturity as a Proxy for Frictional Fault Heating: Experimental Constraints on Methylphenanthrene Kinetics at Earthquake Timescales. *Geochimica et Cosmochimica Acta* 151: 103–16. https://doi.org/10.1016/j.gca.2014.11.020.

Siman-Tov, S., Aharonov, Sagy, A. and Emmanuel, S. (2013). Nanograins Form Carbonate Fault Mirrors. *Geology* 41 (6): 703–6. https://doi.org/10.1130/G34087.1.

Siman-Tov, S., Aharonov, E., Boneh, Y. and Reches, Z. (2015). Fault Mirrors along Carbonate Faults: Formation and Destruction during Shear Experiments. *Earth and Planetary Science Letters* 430: 367–76. https://doi.org/10.1016/j.epsl.2015.08.031.

Smith, S. A. F., Di Toro, G., Kim, S., Ree, J. H., Nielsen, S., Billi, A. and Spiess, R. (2013). Coseismic Recrystallization during Shallow Earthquake Slip. *Geology* 41 (1): 63–66. https://doi.org/10.1130/G33588.1.

Spagnuolo, E., Plümper, O., Violay, M., Cavallo, A. and Di Toro. G. (2015). Fast-Moving Dislocations Trigger Flash Weakening in Carbonate-Bearing Faults during Earthquakes. *Scientific Reports* 5: 1–11. https://doi.org/10.1038/srep16112.

Suchy, V., Frey, M. and Wolf, M. (1997). Vitrinite reflectance and shear- induced graphitization in orogenic belts: a case study from the Kandersteg area, Helvetic Alps, Switzerland. *International Journal of Coal Geology* 34, 1–20.

Sweeney, J. J. and Burnham, A. K. (1990). Evaluation of a Simple Model of Vitrinite Reflectance Based on Chemical Kinetics. *AAPG Bulletin,* 74 (10): 1559–1570. https://doi.org/10.1306/0C9B251F-1710-11D7-8645000102C1865D.

Tesei, T., Carpenter, B. M., Giorgetti, C., Scuderi, M. M., Sagy, A., Scarlato, P. and Collettini, C. (2017). Friction and Scale-Dependent Deformation Processes of Large Experimental Carbonate Faults. *Journal of Structural Geology* 100: 12–23. https://doi.org/10.1016/j.jsg.2017.05.008.

Tisato., N., Di Toro, G., De Rossi, N., Quaresimin, M. and Candela, T. (2012). Experimental Investigation of Flash Weakening in Limestone. *Journal of Structural Geology* 38: 183–99.

https://doi.org/10.1016/j.jsg.2011.11.017.

Tissot, B.P. and Welte, D.H. (1984). Petroleum Formation and Occurrence. 2nd Edition, *Springer-Verlag*.

Verberne, B. A., Spiers, C. J., Niemeijer, A. R., De Bresser, J. H.P., De Winter, D. A.M. and Plümper, O. (2014). Frictional Properties and Microstructure of Calcite-Rich Fault Gouges Sheared at Sub-Seismic Sliding Velocities. *Pure and Applied Geophysics* 171 (10): 2617–40. https://doi.org/10.1007/s00024-013-0760-0.

Figure 2

Click here to access/download;Figure;Figure2.tiff

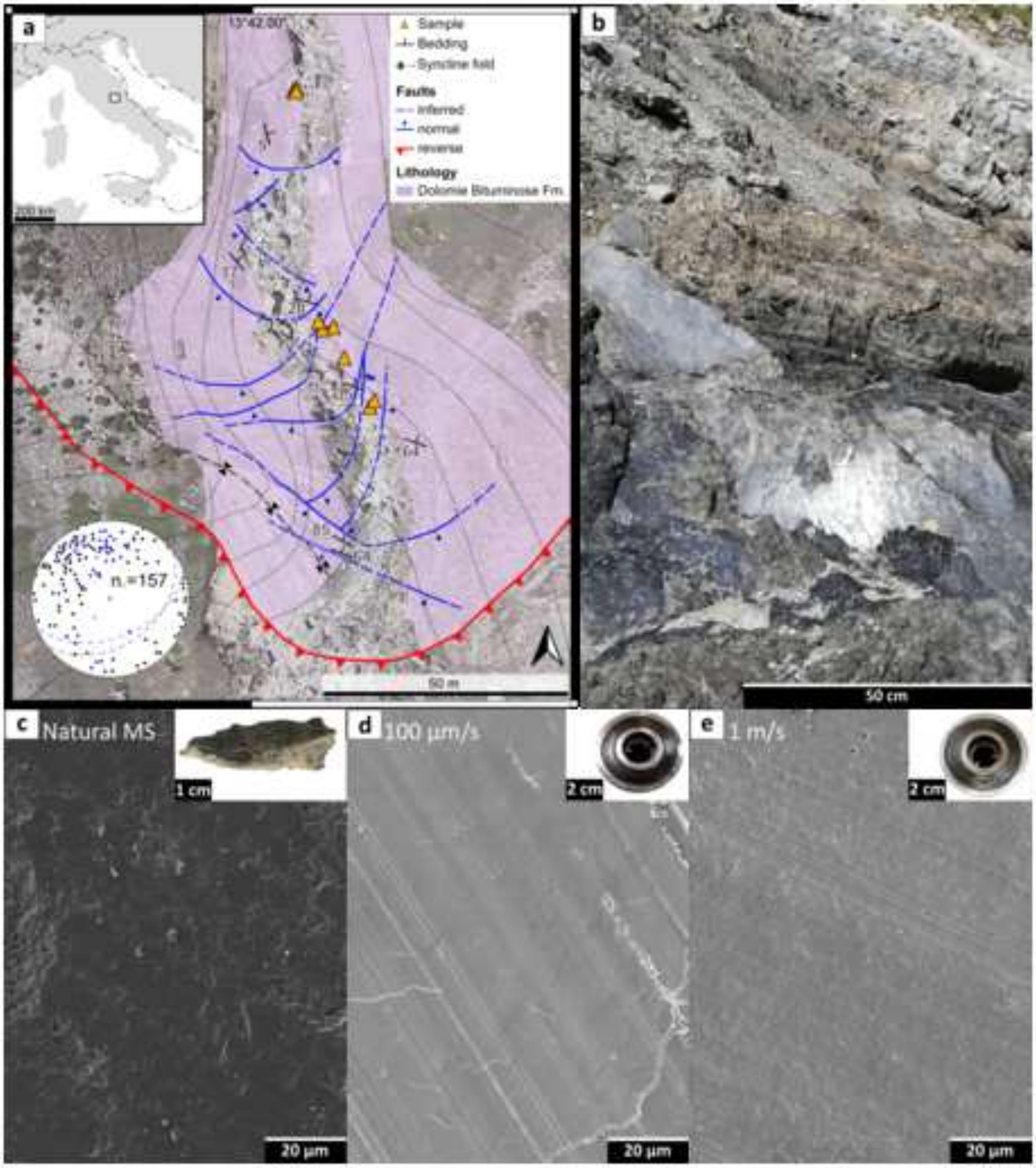

Figure 1

Click here to access/download;Figure;Figure1.tiff

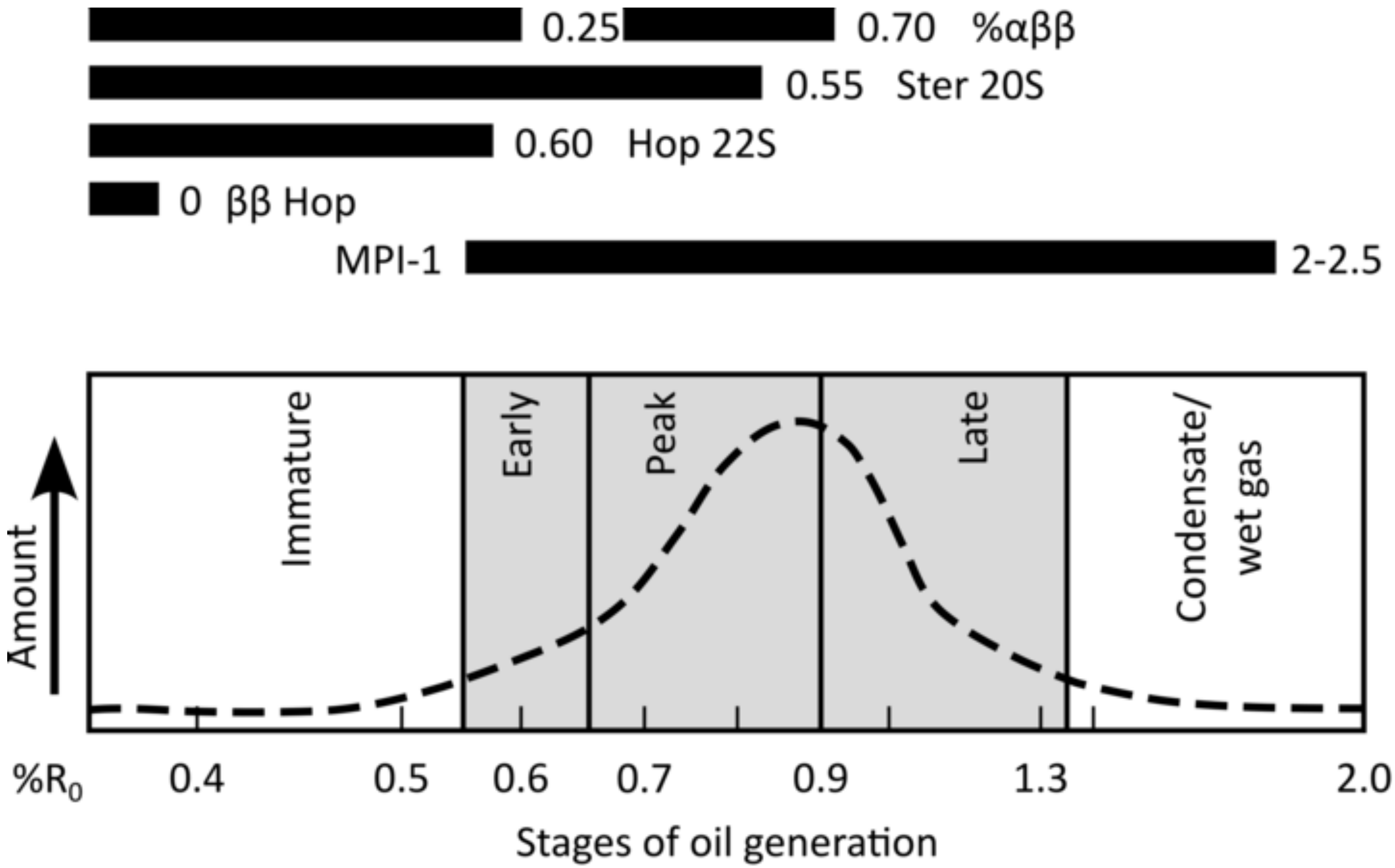

Figure 7

Click here to access/download;Figure;Figure7.tiff

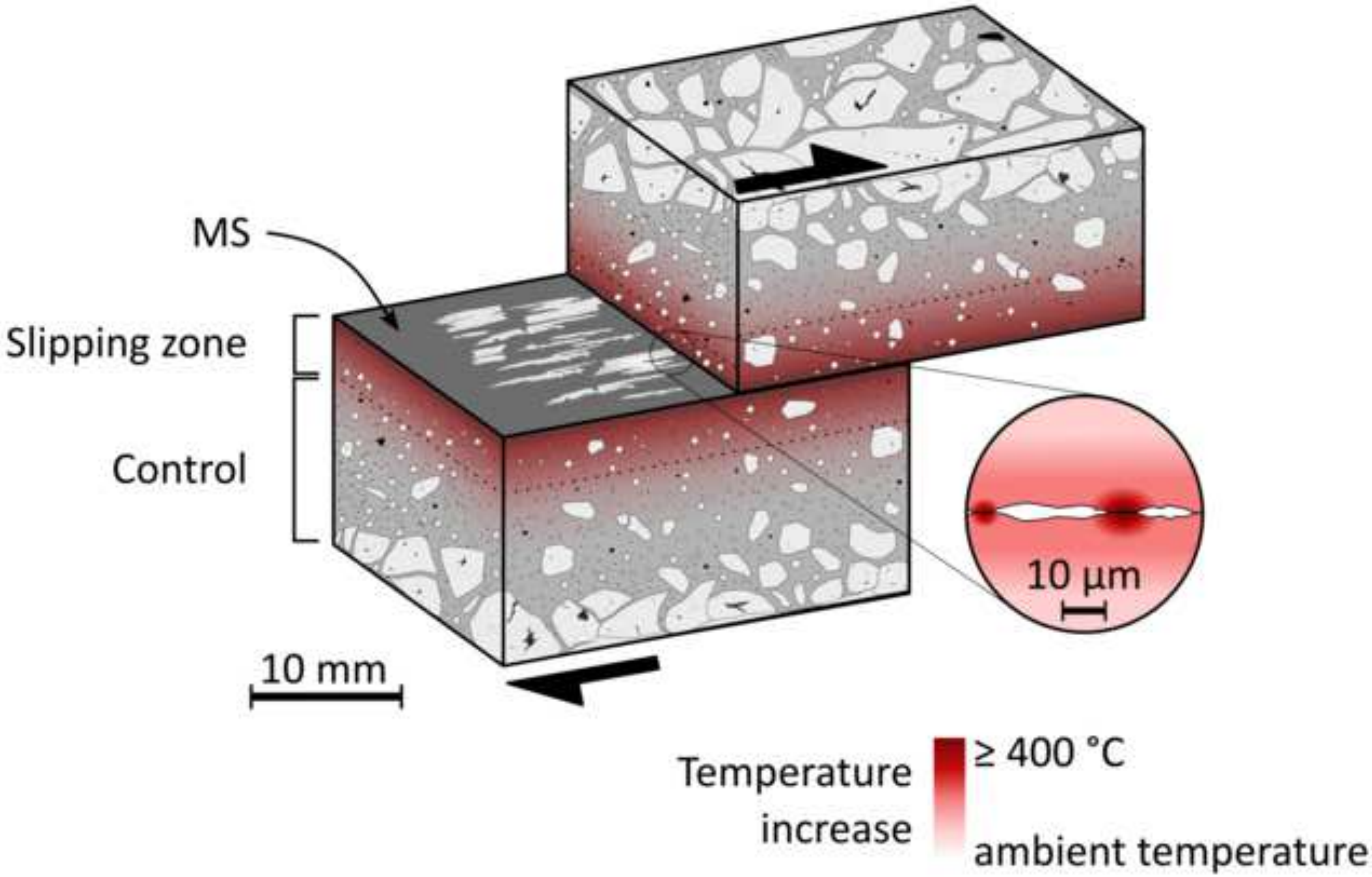

Figure 6

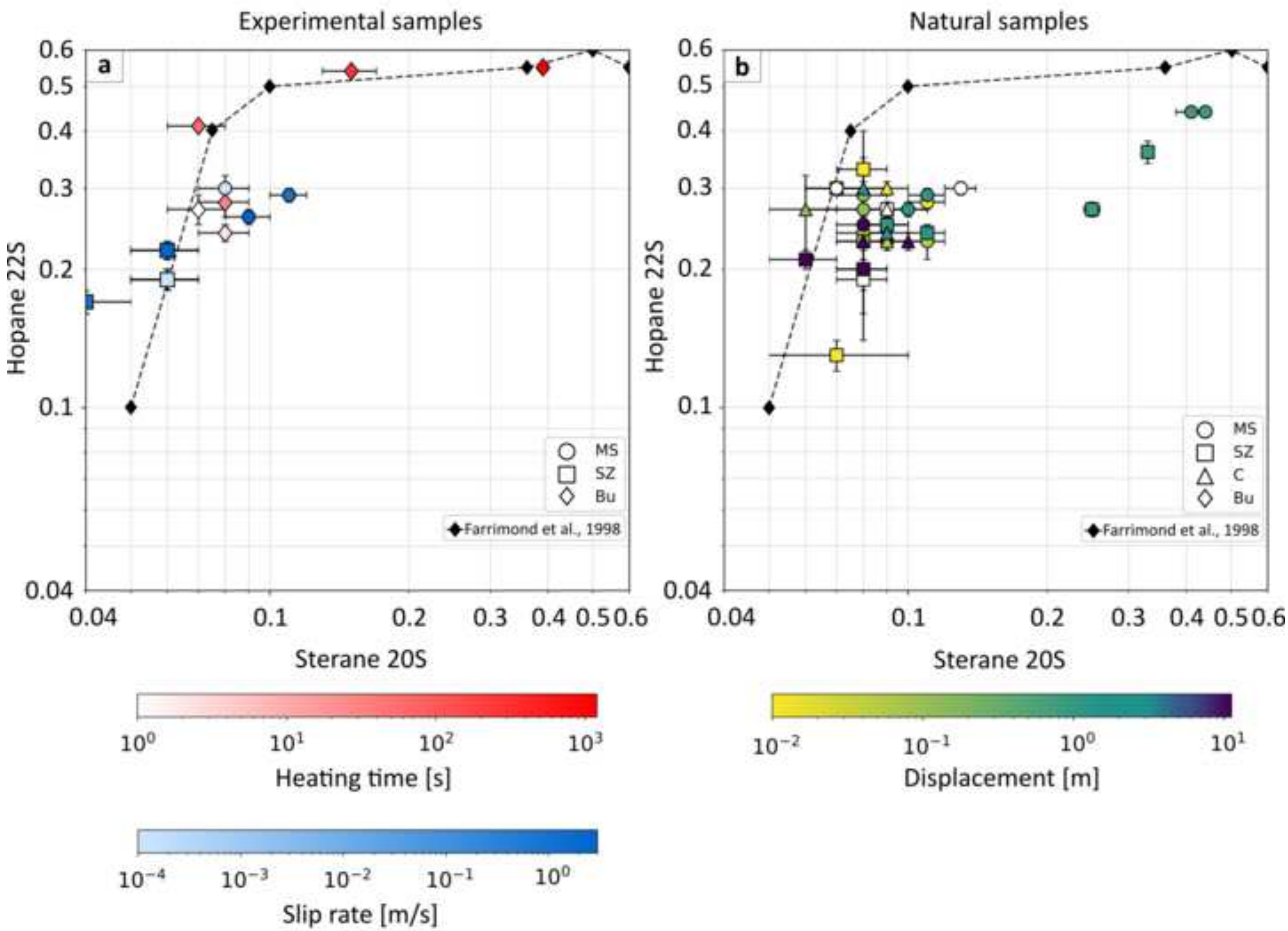

Experimental samples
a
Hopane 22S
0.6
0.5
0.4
0.3
0.2
0.1
0.04
Sterane 20S
0.04
0.1
0.2
0.3
0.4
0.5
0.6
MS
SZ
Bu
Farrimond et al., 1998
Heating time [s]
10^0
10^1
10^2
10^3
Slip rate [m/s]
10^{-4}
10^{-3}
10^{-2}
10^{-1}
10^0
Natural samples
b
MS
SZ
C
Bu
Farrimond et al., 1998
Displacement [m]
10^{-2}
10^{-1}
10^0
10^1

Figure 5

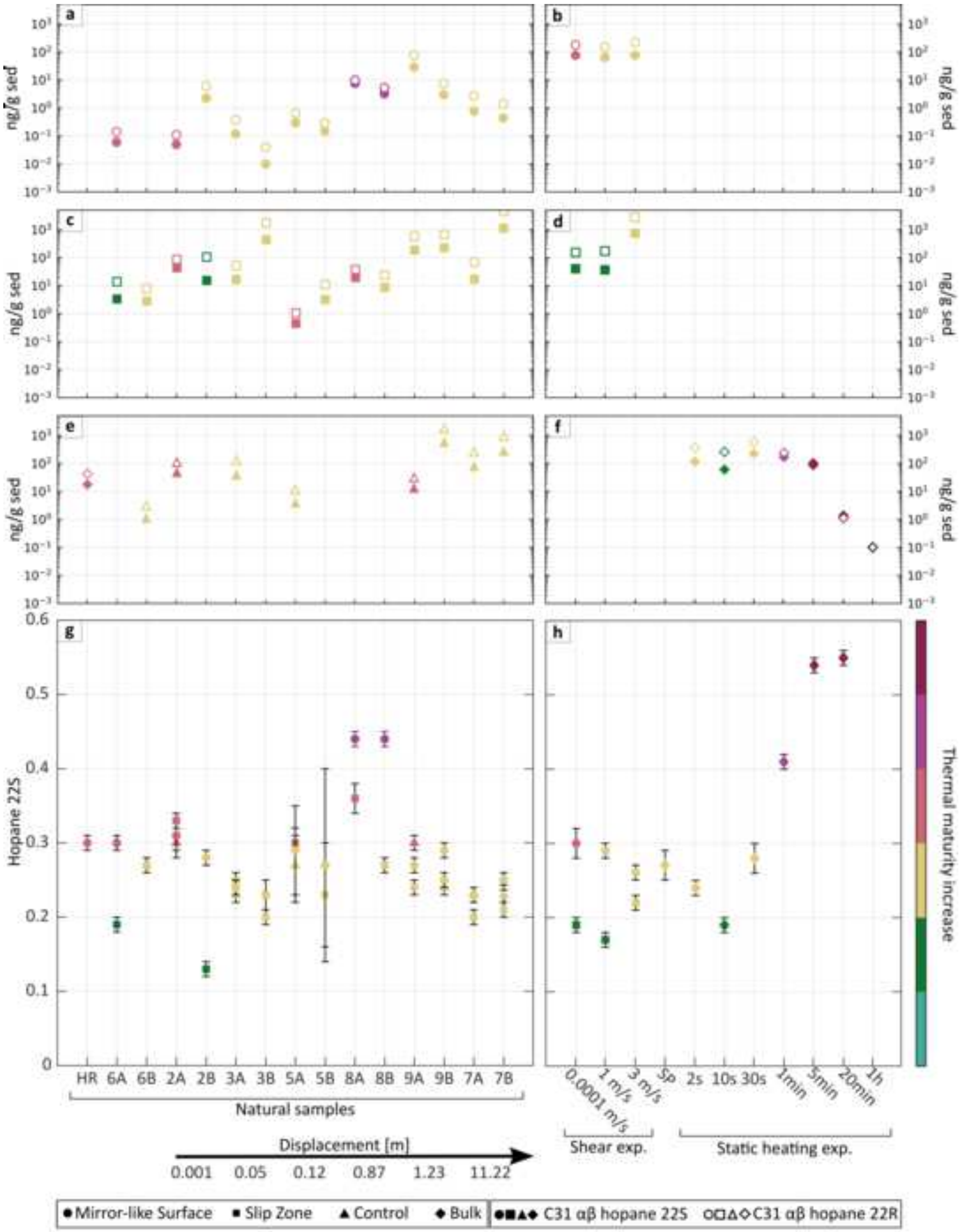
a
b
c
d
e
f
g
h
ng/g sed
Hopane 22S
HR 6A 6B 2A 2B 3A 3B 5A 5B 8A 8B 9A 9B 7A 7B
Natural samples
0.0001 m/s 1 m/s 3 m/s Sp 2s 10s 30s 1min 5min 20min 1h
Shear exp.
Static heating exp.
Thermal maturity increase
Displacement [m]
0.001 0.05 0.12 0.87 1.23 11.22
Mirror-like Surface
Slip Zone
Control
Bulk
C31 αβ hopane 22S
C31 αβ hopane 22R

Figure 4

Click here to access/download;Figure;Figure4.tiff

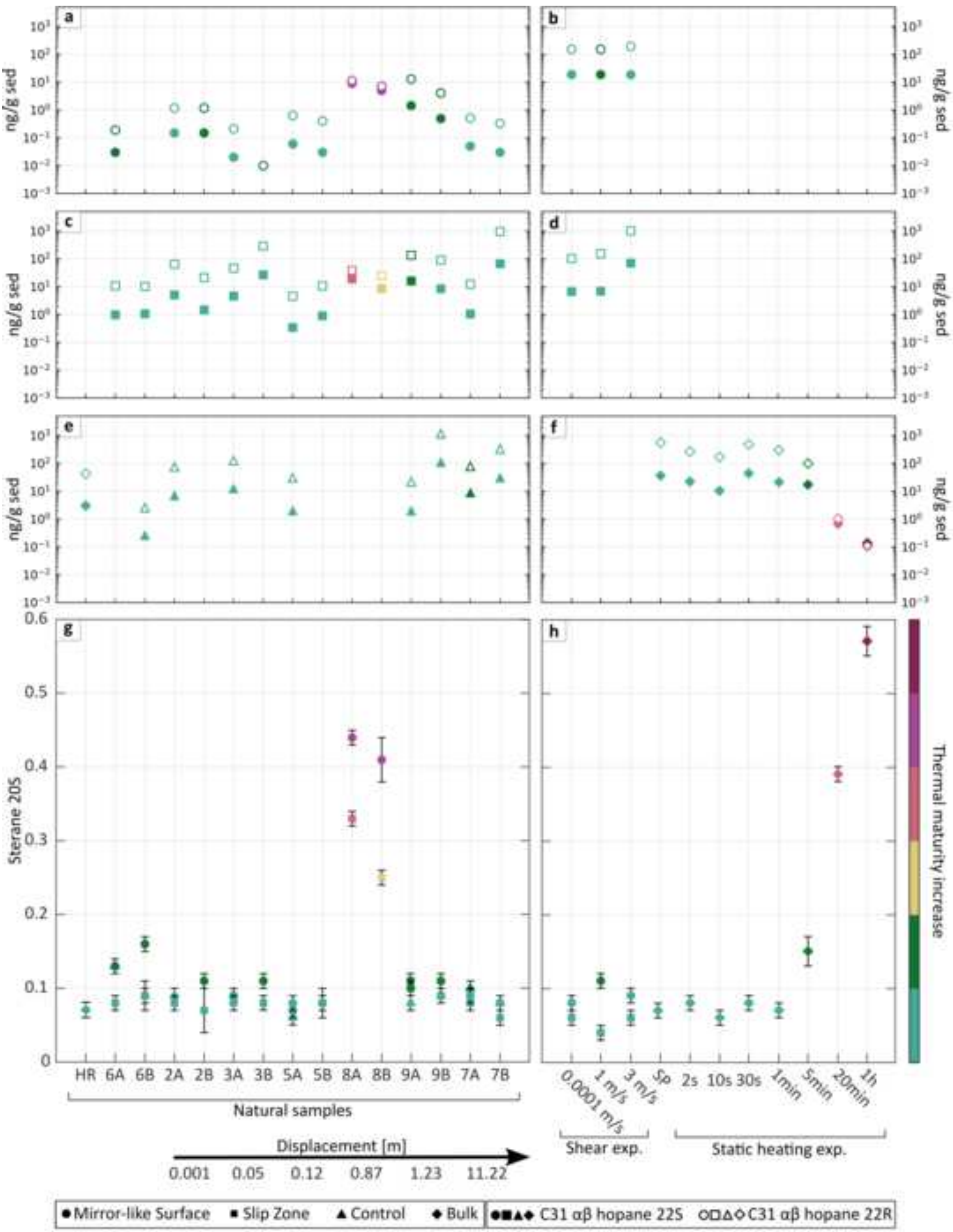

Figure 3

Click here to access/download;Figure;Figure3.tiff

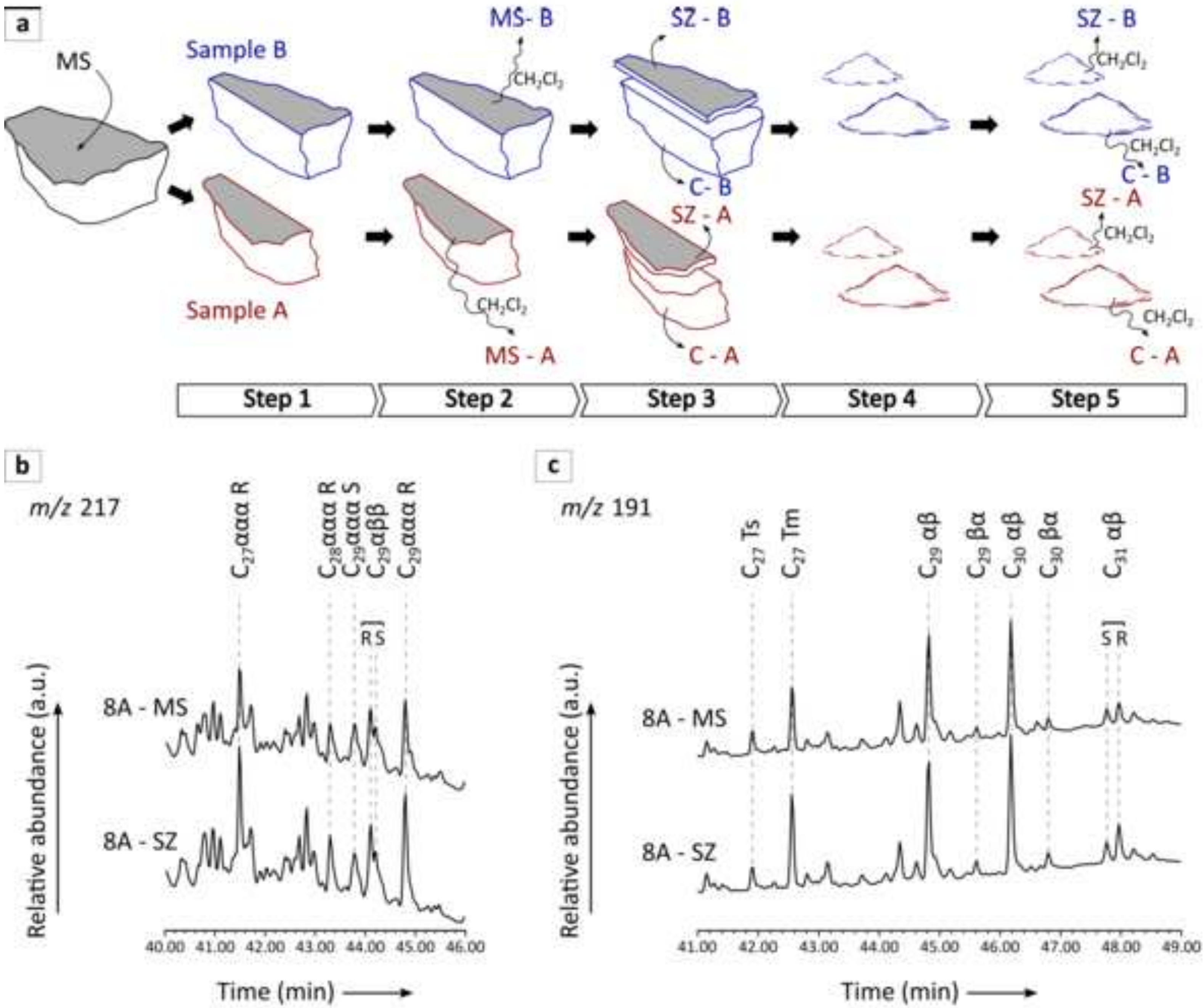

Figure Captions

Figure 1. Thermal maturity equivalence of the biomarker parameters tested in this study compared to stages of oil generation, and Vitrinite reflectance (Ro%). The tested biomarker parameters are steranes (*%αββ* sterane and sterane 20S), hopanes (hopane 22S and *ββ* hopane) and the methylphenanthrene index (MPI-1; see Supporting Information). Grey areas correspond to the "oil window," while black bars represent the range of each biomarker parameter and the maximum value that normally does not change with further maturity. *ββ* hopane (hop) parameter decreases to 0 with increasing thermal maturity, while the values of the other parameters increase with thermal maturity. For the *%αββ* sterane parameter an intermediate value is shown within the bar to indicate earlier stages of maturity. Modified after Peters and Moldowan (2017).

Figure 2. Structural map of the Fornaca Valley (Gran Sasso Massif, Central Apennines, Italy) and analyzed fault samples. **(a)** Structural map of the surveyed area. The bituminous dolostones (in pale violet color) crop out in the footwall of the Monte Camicia Thrust (red curve). Stereoplot shows poles to measured faults (blue for normal faults, red for reverse faults and black for faults with uncertain kinematics) and dashed lines represent mean fault surfaces orientation. Inset in the upper-left corner shows the location of the study area within the structural frame of Italy. Modified after Chinello et al. (2023). **(b)** Mirror-like Surface (MS) cutting the bituminous dolostones. **(c)**, **(d)**, **(e)** SEM-SE images of a natural MS and of two experimental MSs obtained at (d) 100 µm/s and (e) 1 m/s (Chinello et al., under review).

Figure 3. Sketch showing the bitumen extraction process for GC-MS analysis and example ion chromatograms. **(a)** Natural fault samples bound by a Mirror-like Surface (MS) were divided into part A and B (step 1) and for every part bitumen was extracted from the MS using dichloromethane (CH_2Cl_2; step 2). Then the slip zone (SZ) containing the MS was separated from the underlying "control" part (C) with a saw (step 3) and every part was crushed (step 4) for bitumen extraction (step 5). **(b)** Example m/z 217 ion chromatograms of bitumen extracted from the MS and SZ of sample 8A showing the distribution of sterane biomarkers; C29 ααα S = 5α,14α,17α (H) 20S sterane; C29 αββ S = 5α,14β,17β (H) 20S sterane. **(c)** Example m/z 191 ion chromatograms of bitumen extracted from the MS and SZ of sample 8A showing the distribution of hopane biomarkers; C27 Ts = C27 18α(H)-22,29,30 trisnorneohopane; C27 Tm = C27 17α(H)-22,29,30 trisnorhopane; C30 αβ = C30 17α,21β(H) hopane; C30 βα = C30 17β,21α (H) hopane/moretane; C31 αβ S= C31 17α,21β(H) 22S homohopane.

Figure 4. Values with the associated standard deviation of sterane 20S thermal maturity parameters and yields of the relative sterane 20S and 20R isomers for all the analyzed samples. **(a)**, **(c)** and **(e)** show the concentrations in the natural samples and the host rock, while **(b)**, **(d)** and **(f)** show the concentrations in the shear- and static-heating experimental samples. **(g)** shows the sterane 20S thermal maturity values for the natural samples, while **(h)** shows the sterane 20S thermal maturity values for the shear and static-heating experimental samples. Dots, squares and triangles represent the values of the MSs, slip zones containing a MS (analyzed after MS bitumen extraction), and the control part (i.e., the furthest part of the sample from the MS), respectively. Diamonds represent the bulk thermal maturity values of the Host Rock sample (HR) in (e) and (g), and of the heated bituminous dolostone powders in (f) and (h). Colors indicate increasing thermal maturity in all graphs. In (g) the black arrow at the top of the graph indicates increasing displacement from left to right. SP = Starting Powder.

Figure 5. Values with the associated standard deviation of hopane 22S thermal maturity parameters and yields of the relative hopane 22S and 22R isomers for all the analyzed samples. **(a)**, **(c)** and **(e)** show the concentrations in the natural samples and the host rock, while **(b)**, **(d)** and **(f)** show the concentrations in the shear- and static-heating experimental samples. **(g)** shows the hopane 22S thermal maturity values for the natural samples, while (h) shows the hopane 22S thermal maturity values for the shear and static-heating experimental samples. Dots, squares and triangles represent the values of the MSs, slip zones containing a MS (analyzed after MS bitumen extraction), and the control part (i.e., the furthest part of the sample from the MS), respectively. Diamonds represent the bulk thermal maturity values of the Host Rock sample (HR) in (e) and (g), and of the heated bituminous dolostone powders in (f) and (h). Colors indicate increasing thermal maturity in all graphs. In (g) the black arrow at the top of the graph indicates increasing displacement from left to right. Note that in (f) the concentration of the Starting Powder (SP) is out of scale.

Figure 6. Log-log plots showing sterane 20S vs hopane 22S thermal maturity values of experimental and natural samples. **(a)** Sterane 20S vs hopane 22S thermal maturity values with the associated standard

deviation for static-heating and rotary-shear experimental samples. Red to white color bar = heating time for the static heating experiments; white to blue color bar = slip rate for the rotary-shear experiments. **(b)** Sterane 20S vs hopane 22S thermal maturity values with the associated standard deviation for the natural samples. Color bar = total displacement accumulated by each fault. In both plots: bulk analyses (for the static-heating experiments and for the starting material) = diamonds, Mirror-like Surface (MS) = dots; Slip Zone (SZ) = squares, Control part (C) = triangles; black diamonds (linked by a dashed line) = trend in thermal maturity during burial (Farrimond et al., 1998).

Figure 7. Sketch showing frictional heating in a slip zone in bituminous dolostones bounded by a Mirror-like Surface (MS) during seismic slip. Frictional heating can cause a temperature increase in the slip surface or localized at the asperity contacts (see inset) depending on the surface roughness. The temperature decreases rapidly away from the MS together with the thermal maturity of bitumen found both in the clast pores and free in the matrix. Thermal maturity of the control part approximates the background thermal maturity of the host rock. Red color bar = expected temperature in the slip zone.